2016

The Sanandaj-Sirjan Zone in the Neo-Tethyan suture, western Iran: Zircon U-Pb evidence of late Palaeozoic rifting of northern Gondwana and mid-Jurassic orogenesis

Chris L. Fergusson
University of Wollongong, cferguss@uow.edu.au

Allen Phillip Nutman
University of Wollongong, anutman@uow.edu.au

Mohammad Mohajjel
Tarbiat Modares University, mohajjel@uow.edu.au

Vickie C. Bennett
Australian National University, vickie.bennett@anu.edu.au

Publication Details

Fergusson, C., Nutman, A. P., Mohajjel, M. & Bennett, V. (2016). The Sanandaj-Sirjan Zone in the Neo-Tethyan suture, western Iran: Zircon U-Pb evidence of late Palaeozoic rifting of northern Gondwana and mid-Jurassic orogenesis. Gondwana Research, 40 43-57.

The Sanandaj-Sirjan Zone in the Neo-Tethyan suture, western Iran: Zircon U-Pb evidence of late Palaeozoic rifting of northern Gondwana and mid-Jurassic orogenesis

Abstract

The Zagros Orogen, marking the closure of the Neo-Tethyan Ocean, formed by continental collision beginning in the late Eocene to early Miocene. Collision was preceded by a complicated tectonic history involving Pan-African orogenesis, Late Palaeozoic rifting forming Neo-Tethys, followed by Mesozoic convergence on the ocean's northern margin and ophiolite obduction on its southern margin. The Sanandaj-Sirjan Zone is a metamorphic belt in the Zagros Orogen of Gondwanan provenance. Zircon ages have established Pan-African basement igneous and metamorphic complexes in addition to uncommon late Palaeozoic plutons and abundant Jurassic plutonic rocks. We have determined zircon ages from units in the northwestern Sanandaj-Sirjan Zone (Golpaygan region). A sample of quartzite from the June Complex has detrital zircons with U-Pb ages mainly in 800-1050 Ma with a maximum depositional age of 547 ± 32 Ma (latest Neoproterozoic¿earliest Cambrian). A SHRIMP U-Pb zircon age of 336 ± 9 Ma from gabbro in the June Complex indicates a Carboniferous plutonic event that is also recorded in the far northwestern Sanandaj-Sirjan Zone. Together with the Permian Hasanrobat Granite near Golpaygan, they all are considered related to rifting marking formation of Neo-Tethys. Scarce detrital zircons from an extensive package of metasedimentary rocks (Hamadan Phyllite) have ages consistent with the Triassic to Early Jurassic age previously determined from fossils. These ages confirm that an orogenic episode affected the Sanandaj-Sirjan Zone in the Early to Middle Jurassic (Cimmerian Orogeny). Although the Cimmerian Orogeny in northern Iran reflects late Triassic to Jurassic collision of the Turan platform (southern Eurasia) and the Cimmerian microcontinent, we consider that in the Sanandaj-Sirjan Zone a tectonothermal event coeval with the Cimmerian Orogeny resulted from initiation of subduction and closure of rift basins along the northern margin of Neo-Tethys.

Disciplines

Medicine and Health Sciences | Social and Behavioral Sciences

Publication Details

Fergusson, C., Nutman, A. P., Mohajjel, M. & Bennett, V. (2016). The Sanandaj-Sirjan Zone in the Neo-Tethyan suture, western Iran: Zircon U-Pb evidence of late Palaeozoic rifting of northern Gondwana and mid-Jurassic orogenesis. Gondwana Research, 40 43-57.

The Sanandaj–Sirjan Zone in the Neo-Tethyan suture, western Iran: zircon U-Pb evidence of late Palaeozoic rifting of northern Gondwana and mid Jurassic orogenesis

C.L. Fergusson[a], A.P. Nutman[a], M. Mohajjel[b], and V.C. Bennett[c]

[a]GeoQuEST Research Centre, School of Earth & Environmental Sciences, University of Wollongong, Wollongong, NSW 2522, Australia
[b]Deceased, formerly Geology Department, University of Tarbiat Modares, P.O. Box 14155-175, Tehran, Iran
[c]Research School of Earth Sciences, Australian National University, Canberra ACT 0200, Australia
Corresponding author – C. L. Fergusson, email: cferguss@uow.edu.au

Abstract: The Zagros Orogen, marking the closure of the Neo-Tethyan Ocean, formed by continental collision beginning in the late Eocene to early Miocene. Collision was preceded by a complicated tectonic history involving Pan-African orogenesis, Late Palaeozoic rifting forming Neo-Tethys, followed by Mesozoic convergence on the ocean's northern margin and ophiolite obduction on its southern margin. The Sanandaj-Sirjan Zone is a metamorphic belt in the Zagros Orogen of Gondwanan provenance. Zircon ages have established Pan-African basement igneous and metamorphic complexes in addition to uncommon late Palaeozoic plutons and abundant Jurassic plutonic rocks. We have determined zircon ages from units in the northwestern Sanandaj-Sirjan Zone (Golpaygan region). A sample of quartzite from the June Complex has detrital zircons with U–Pb ages mainly in 800-1050 Ma with a maximum depositional age of 547±32 Ma (latest Neoproterozoic – earliest Cambrian). A SHRIMP U–Pb zircon age of 336±9 Ma from gabbro in the June Complex indicates a Carboniferous plutonic event that is also recorded in the far northwestern Sanandaj-Sirjan Zone. Together with the Permian Hasanrobat Granite near Golpaygan, they all are considered related to rifting marking formation of Neo-Tethys. Scarce detrital zircons from an extensive package of metasedimentary rocks (Hamadan Phyllite) have ages consistent with the Triassic to Early Jurassic age previously determined from fossils. These ages confirm that an orogenic episode affected the Sanandaj–Sirjan Zone in the Early to Middle Jurassic (Cimmerian Orogeny). Although the Cimmerian Orogeny in northern Iran reflects late Triassic to Jurassic collision of the Turan platform (southern Eurasia) and the Cimmerian microcontinent, we consider that in the Sanandaj-Sirjan Zone a tectonothermal event coeval with the Cimmerian Orogeny resulted from initiation of subduction and closure of rift basins along the northern margin of Neo-Tethys.

Keywords: Carboniferous; Cimmeria; rifting; Sanandaj-Sirjan; zircon.

1. Introduction

Tethys was the major triangular-shaped ocean between Eurasia and Gondwana that existed in the Palaeozoic to Cenozoic and was characterised by ribbon-like continental fragments such as Cimmeria, which rifted away from the northern margin of Gondwana to form Neo-Tethys in the Permian-Triassic (Şengör, 1984; Ricou, 1994; Stampfli and Borel, 2002). In northern Iran, the Palaeo-Tethyan suture is along

the Alborz and Kopet Dagh mountain ranges (Figs. 1, 2) and formed by collision of the Cimmerian continental fragment to the Turan platform of Eurasia in the Late Triassic to Early Jurassic Cimmerian Orogeny (Şengör, 1984; Stampfli and Kozur, 2006; Wilmsen et al., 2009; Zanchi et al., 2015). In southwestern Iran, the Neo-Tethyan suture is along the Main Zagros Thrust in the Zagros Mountains (Zagros Orogen) (Fig. 2), and formed by continental collision in either the late Eocene (Allen and Armstrong (2008) or Oligocene (McQuarrie and van Hinsbergen, 2013). Northeast of the suture is the Sanandaj-Sirjan Zone that consists of basement metamorphic, igneous and sedimentary rocks, interpreted to form the southwestern margin of the Cimmerian continental fragment (Şengör, 1984; Ricou, 1994; Stampfli and Borel, 2002).

The Sanandaj-Sirjan Zone contains scattered elements of Pan-African basement that is widely developed in parts of Iran and Turkey (Hasanzandeh et al, 2008; Nutman et al., 2014). Sparse Late Carboniferous and Permian igneous activity has been more widely reported within the Sanandaj-Sirjan Zone (Figs. 2, 3) and these include A-type plutons south of Lake Urumieh (315±2 Ma; Bea et al., 2011), adjacent to Lake Urumieh (320-317 Ma; Moghadam et al., 2015) and farther southeast in the Golpaygan region (288±4 Ma; Alirezaei and Hassanzadeh, 2012). The Carboniferous-Permian igneous activity preceded and accompanied rifting of the Cimmerian continental fragment away from the northern margin of Gondwana from the Permian onwards (Şengör, 1984; Stampfli and Borel, 2002; Mohajjel et al., 2003; Agard et al., 2011; Alirezaei and Hassanzadeh, 2012; Moghadam et al., 2015; Shakerardakani et al., 2015; Hassanzadeh and Wernicke, 2016).

We present new U-Pb zircon ages from the June Complex and related units in the northwestern part of the Sanandaj-Sirjan Zone (Fig. 2), with the aim of clarifying the evolution of the June Complex and Hamadan Phyllite. We find that the June Complex formed from latest Neoproterozoic to Triassic protoliths, and was subsequently deformed and metamorphosed in the mid Jurassic Cimmerian Orogeny. We also dated zircons from the Hamadan Phyllite to test this idea. We explore the significance of these results for the setting of the Sanandaj-Sirjan Zone in the Palaeozoic and its roles in the Cimmerian continental fragment and subsequent involvement in tectonic events.

2. Geological setting

2.1 Zagros Orogen and the Cimmerian continental fragment

The Zagros Orogen in southwestern to northwestern Iran is divided by the Main Zagros Thrust into the Sanandaj-Sirjan Zone to the northeast and the Zagros Fold and Thrust Belt to the southwest (Alavi, 1994; Agard et al., 2011). The Sanandaj-Sirjan Zone consists of metamorphic, igneous and sedimentary units of late Neoproterozoic to Neogene age in the hanging wall of the Main Zagros Thrust (Alavi, 1994; Mohajjel et al., 2003; Agard et al., 2005, 2011; Mohajjel and Fergusson, 2014; Mehdipour Ghazi and Moazzen, 2015; Shakerardakani et al., 2015; Sheikholeslami, 2015). The Zagros Fold and Thrust Belt has a Phanerozoic succession deformed during the late Eocene to present continental collision between Eurasia and the Arabian continent (Hessami et al., 2001; Alavi, 2004). Associated with the northeast-dipping Main Zagros Thrust are Cretaceous ophiolites, Mesozoic limestones and radiolarites, along the suture between the northwestern Arabian margin and the Sanandaj-Sirjan Zone (Mohajjel et al., 2003; Agard et al., 2005, 2011; Moghadam

and Stern, 2011). Abundant Eocene volcanic rocks of the Urumieh-Dokhtar Magmatic Arc occur northeast of the Sanandaj-Sirjan Zone (Fig. 2) and reflect subduction of Neo-Tethyan oceanic crust prior to collision (Alavi, 1994; Agard et al., 2011; Verdel et al., 2011). Volcanic rocks of a similar age are widely distributed throughout most of the rest of Iran east and north of the Urumieh-Dokhtar Magmatic Arc (Verdel et al., 2011).

The Sanandaj-Sirjan Zone has been interpreted as the southwestern fringe of the Cimmerian continental fragment (Şengör, 1984; Ricou, 1994; Stampfli and Borel, 2002). However, the idea of a single Iranian Cimmerian continent requires reassessment, given evidence for Late Palaeozoic and Triassic to mid Jurassic events within it. The Triassic-Jurassic Palaeo-Tethyan suture has been identified within the Yazd Block of Central Iran (Fig. 2); well south of the main strand of the suture in the Alborz and Kopet Dagh mountains (Bagheri and Stampfli, 2008). Carboniferous accretion (Variscan) at the northern margin of Palaeo-Tethys, prior to the collision within the Yazd Block, has been determined from radiometric ages on metamorphic rocks (Bagheri and Stampfli, 2008; Zanchi et al., 2009, 2015). Palaeomagnetic data show that the various blocks of Central Iran have undergone considerable counter-clockwise rotations in the Late Jurassic and Neogene so that their present-day configuration differed considerably to that in the Palaeozoic and early Mesozoic (Mattei et al., 2012, 2015).

2.2 June Complex and Hamadan Phyllite

Within the Sanandaj-Sirjan Zone, crystalline rocks include inliers northeast of Golpaygan (Fig. 3) containing metamorphic rocks that are intruded by variably deformed granites with zircon ages of 578±22 Ma, 596±24 Ma, 588 ± 23 Ma and are part of the Pan-African basement of the Sanandaj-Sirjan Zone (Hassanzadeh et al., 2008; Moosavi et al., 2014). The Galeh-Doz Orthogneiss, northwest of Azna (Figs. 3, 4), has an U-Pb zircon age of 568±11 Ma (Nutman et al., 2014), and additional ages of 608±18 Ma and 588±41 Ma have been found from nearby lenses of granitic orthogneiss (Shakerardakani et al., 2015). Previously, the Galeh-Doz Orthogneiss was regarded as Late Cretaceous (Mohajjel and Fergusson, 2000; Mohajjel et al., 2003). The Pan-African Galeh-Doz Orthogneiss is an A-type granite that is intensely deformed, but no contact metamorphic aureole has been identified in the adjacent June Complex (Shabanian et al., 2009).

Northwest of Azna (Fig. 4), the June Complex consists of intensely deformed marble, dolomite, schist, amphibolite, mafic schist, and quartzite (Mohajjel and Fergusson, 2000). Dolomite and marble within regional equivalents of the June Complex contain Triassic fossils (Shakerardakani et al., 2015), but other lithologies such as amphibolite, quartzite and schist lack age control. A metagabbro sample from within the June Complex has a U-Pb zircon age of 315±4 Ma and massive gabbro intrusive into schist has a U-Pb zircon age of 170±3 Ma (Shakerardakani et al., 2015). Metagabbro and amphibolites of the June Complex have a tholeiitic geochemical affinity consistent with E-MORB and N-MORB and have been interpreted as related to rifting (Shakerardakani et al., 2015). A stock of massive gabbro has intruded the June Complex southeast of Meydanak village (Fig. 4). In the Azna region (Fig. 4), the amphibolite to upper greenschist Pan-African and younger metamorphic rocks are thrust to the southwest over weakly metamorphosed Upper Jurassic to Cretaceous andesitic volcanic rocks and limestone (Mohajjel, 1997; Mohajjel and Fergusson, 2000).

Northeast of the June Complex is the Triassic to Lower Jurassic Hamadan Phyllite (Fig. 3), a widespread unit that consists of dominantly black phyllite and minor lithic sandstone in a thick succession of turbidites (Mohajjel et al., 2003). Locally, fossils in slates in the Hamadan region indicate an early Middle Jurassic age (Baharifar et al., 2004). In the Hamadan region, the Hamadan Phyllite is strongly deformed with widespread schists of amphibolite to greenschist facies grade including sillimanite, garnet, staurolite and andalusite-bearing assemblages and cordierite in contact aureoles (Baharifar et al., 2004). Metamorphic and associated plutonic rocks have common K-Ar ages in the range 150-60 Ma indicative of cooling in the Cretaceous to early Palaeogene (Baharifar et al., 2004). However, it has been determined that the Alvand plutonic complex in the Hamadan region has numerous U-Pb zircon ages in the range 167-153 Ma (Shahbazi et al., 2010; Mahmoudi et al., 2011). These plutonic rocks intruded the crystalline schists in the Hamadan region, which are therefore pre-mid Jurassic (Mahmoudi et al., 2011; Mohajjel and Fergusson, 2014). The widespread Jurassic calc-alkaline igneous rocks of the Sanandaj-Sirjan Zone are consistent with its development as an elongate magmatic arc along the southwestern margin of Central Iran (Mahmoudi et al., 2011; Mohajjel and Fergusson, 2014). Elsewhere in Iran, Early to Middle Jurassic deformation is attributed to the Cimmerian Orogeny (Sheikoleslami et al., 2008; Sheikholeslami, 2015).

2.3 *Structure of the June Complex in the June area*

The detailed structure of the June Complex and associated units in the June (Zhan) area has been presented by Mohajjel (1997), Mohajjel and Fergusson (2000) and the following summary is based on this work with minor revisions by Mohajjel and Fergusson (2014) and Shakerardakani et al. (2015). The metamorphic rocks are multiply deformed with two main phases of deformation. The first deformation (D_1) has formed F_1 folds and associated axial planar foliation (S_1) that are locally northeast-trending but are only recognised in a few areas especially where the lower quartzite unit is thickest (Fig. 4). These F_1 folds are strongly overprinted and refolded by the dominant D_2 deformation that has formed abundant WNW-ESE trending F_2 folds, thrust faults and associated axial planar foliation (S_2). In the June Complex, this deformation has formed a major F_2 antiform-synform couple in the southeast that to the northwest of the area gives way to a major F_2 antiform with a core of amphibolite, mafic and silicic intrusive rocks (Fig. 4).

The Galeh-Doz Orthogneiss and amphibolites in the core of the major F_2 antiform north of Meydanak (Fig. 4) are mylonitised with strong foliation and lineation. The foliation is considered S_2 and continuous with S_2 schistosity in neighbouring schists and carbonates. In contrast to the schists and carbonates, these mylonitic rocks have a strong gently plunging lineation to the northwest and southeast as well as shear sense criteria indicating dextral shear (Mohajjel and Fergusson, 2000). These relationships were interpreted to reflect dextral transpression with partitioning of deformation into two types of domains: (1) domains of schist and marble containing folds and associated thrust faults formed by pure-shear with down-dip extension, and (2) domains of mylonitic rocks (Galeh-Doz Orthogneiss, amphibolite and some calcite mylonite) produced by deformation with a strong component of horizontal simple shear.

To the north and northeast of June (Zhan), the metamorphic rocks of the June Complex and the Permian Kuh-e-June Metacarbonate are thrust over

weakly metamorphosed Upper Jurassic to Cretaceous intermediate volcanic rocks and limestone (Mohajjel and Fergusson, 2000). These thrust faults are associated with the topography and are related to the Cenozoic continental collision (Mohajjel and Fergusson, 2014).

3. Methods

3.1 Sample preparation

Zircon was concentrated using heavy liquid and isodynamic separation techniques at the mineral separation laboratory of the Research School of Earth Sciences, the Australian National University (ANU). Using a binocular microscope, concentrates were hand-picked and selected grains along with reference Temora zircons (Black et al., 2003), were cast in epoxy resin discs, which were ground to a mid-section level through the grains and were then polished. Cathodoluminescence (CL) imaging was used to document the grains (Fig. 5).

3.2 U-Pb geochronology

U-Th-Pb zircon analyses were undertaken with the SHRIMP-2 instrument at the Australian National University (Table 1) following analytical protocols of Williams (1998), with the raw data being reduced using ANU software 'PRAWN' and 'Lead'. Measurements of $^{206}Pb/^{238}U$ in unknown zircons were calibrated using the Temora standard (U-Pb ages concordant at 417 Ma; Black et al., 2003). The reference zircon SL13 (U=238 ppm) located in a set-up mount was used to calibrate U and Th abundance in unknown zircons. The ISOPLOT program (Ludwig, 2003) was used to assess and plot the reduced and calibrated data. $^{206}Pb/^{238}U$ ratios were used to calculate Neoproterozoic and younger U-Pb ages (<1000 Ma), whereas for older zircons the $^{207}Pb/^{206}Pb$ age was used. These older grains have a larger amount of accrued radiogenic ^{207}Pb and thus these ages are more precise than the $^{206}Pb/^{238}U$ ages. Pooled weighted mean ages are rounded to the nearest million years. Ages were corrected for common Pb using measured ^{204}Pb and the Cumming and Richards (1975) Pb composition approximate for the age of the sample. The amount of common Pb was small in all samples (f^{206}(%) always <1%; Table 1).

3.3 Lu-Hf isotopes

Zircon hafnium isotopic compositions were determined over a single analytical session using the RSES ThermoFinnigan Neptune multi-collector ICPMS coupled to a ArF λ=193 nm eximer 'HelEx' laser ablation system following methods described by Hiess et al. (2009). Except from where indicated in Table 2, Hf isotope analytical sites coincided with the U-Pb age determination sites. Owing to the small size of some of the zircons, the laser was focused to a 37 μm diameter circular spot firing at 5 Hz with an energy density at the sample surface of ~10 J/cm2. ^{171}Yb, ^{173}Yb, ^{174}Hf, ^{175}Lu, ^{176}Hf, ^{177}Hf, ^{178}Hf, ^{179}Hf and ^{181}Ta isotopes were simultaneously measured in static-collection mode on 9 Faraday cups with 10^{11} Ω resistors. A large zircon crystal from the Monastery kimberlite was used to tune the mass spectrometer to optimum sensitivity. Analysis of a gas blank and a suite of 6 secondary reference zircons (Mud Tank, QGNG, Plesovice, Temora-2, R-33 and FC1) were performed systematically after every 10-12 sample spot analyses.

Data were acquired in 1 s integrations over 100 s or until the grain burned through. Time slices were later cropped to periods maintaining steady $^{176}Hf/^{177}Hf$ signals during data reduction on a custom Excel™ spreadsheet. Data reduction incorporated a dynamic amplifier correction within run. Total Hf signal intensity typically fell from >12 to ~6 volts during a single analysis. The segmental processing of the laser ablation data means that any down-hole variation in Lu/Hf and $^{176}Hf/^{177}Hf$ ratio can be detected and tracked. In all analyses Lu/Hf and $^{176}Hf/^{177}Hf$ ratios were uniform throughout data acquisition.

The measured $^{176}Lu/^{177}Hf$ and $^{176}Hf/^{177}Hf$ ratios with 2σ uncertainties for each of the sample analyses are presented in Table 2. Based on results from the reference zircons, which were all within error of accepted solution values (Supplementary Table 1), no corrections to the measured $^{176}Hf/^{177}Hf$ were required. Mass bias was corrected using an exponential law (Russell et al., 1978; Chu et al., 2002; Woodhead et al., 2004) and a composition for $^{179}Hf/^{177}Hf$ of 0.732500 (Patchett et al., 1981). As a quality check of this procedure, $^{178}Hf/^{177}Hf$ ratios for all zircon reference materials and samples were monitored and are reported (Supplementary Tables 1 and 2). Yb and Lu mass bias factors were assumed to be identical and normalized using an exponential correction referenced to a $^{173}Yb/^{171}Yb$ ratio of 1.129197 (Vervoort et al., 2004). The intensity of the ^{176}Hf peak was determined accurately by removing isobaric interferences from ^{176}Lu and ^{176}Yb. Interference-free ^{175}Lu and ^{173}Yb were measured and the interference peaks subtracted according to reported $^{176}Lu/^{175}Lu$ and $^{176}Yb/^{173}Yb$ isotopic abundances of Vervoort et al. (2004).

Zircon $^{176}Lu/^{177}Hf$ ratios should be accurately determined by LA-MC-ICPMS, to enable corrections for in-growth of radiogenic ^{176}Hf. Average measured $^{176}Lu/^{177}Hf$ ratios within the reference zircons are in good agreement with the accepted solution values (Supplementary Table 1). No correlation exists between $^{176}Hf/^{177}Hf$ and $^{178}Hf/^{177}Hf$, $^{174}Hf/^{177}Hf$ or $^{176}Lu/^{177}Hf$ ratios for any zircon reference materials, including high Lu/Hf ratio Temora-2 and FC1. This indicates that calculations for mass bias and Yb interference corrections were applied accurately. For the unknown zircons, initial $^{176}Hf/^{177}Hf$ ratios for each spot were calculated using their individual SHRIMP measured U-Pb ages, present day CHUR compositions of $^{176}Hf/^{177}Hf = 0.282785\pm11$, $^{176}Lu/^{177}Hf = 0.0336\pm1$ (Bouvier et al., 2008), and a $\lambda^{176}Lu$ decay constant of $1.867\pm8 \times 10^{-11} y^{-1}$ (Scherer et al., 2001; Söderlund et al., 2004).

4. Results

4.1 U-Pb geochronology

Results from this study and the ages given by Nutman et al. (2014) and Shakerardakani et al. (2015) are summarised in Table 3. Sample P17 is a quartzite sample collected from west-northwest of Meydanak (Fig. 4) and is representative of this rock type in the June Complex. Quartzite sample P17 yielded zircons that are overall small (150-50 μm across), with varied morphology. Some grains are oval, with oscillatory zoning truncated at their margins, whereas others are slightly rounded prisms, with oscillatory zoning more or less parallel to the grain exteriors (Fig. 5A). The grains thus appear to have experienced variable degrees of abrasion in the sedimentary system. Twenty-one analyses were undertaken on 21 grains. Most analyses have high Th/U ratios (0.24 to 1.1) which combined with the widespread preservation of oscillatory zoning shows derivation from igneous

sources. The exception is grain #5, which is dark and homogeneous in the CL image with a Th/U ratio of 0.03, suggestive of derivation from a metamorphic rock. In this case, the age of 594 Ma reflects the timing of zircon recrystallisation, during metamorphism. Most analyses have U-Pb ages indistinguishable from Concordia, with a range of ages from 2493 Ma (grain #4) to a weighted mean $^{206}Pb/^{238}U$ age of 547±32 Ma (95% confidence, MSWD<0.01) for grains #7 and 12 (indistinguishable from the Ediacaran-Cambrian boundary). This gives the maximum age of deposition as latest Neoproterozoic to earliest Cambrian. Other ages for detrital zircons are ~620, 910, 1050 and 1700 Ma (Fig. 6). It is noted that the degree of rounding and truncation of internal oscillatory zoning by sedimentary abrasion is not correlated with increasing age. Thus the two youngest grains (#7 and 12; Fig. 5) are rounded.

Sample 813 is an amphibolite derived from gabbro or dolerite located north of Meydanak (Fig. 4). This sample gave a low yield of small zircons. Most grains are prisms or fragments of prisms, typically 100-50 µm long. In CL images the grains are dominated by igneous-style oscillatory zoning, but overprinted by recrystallisation domains, and commonly have narrow fringes that appear bright in CL images (Fig. 5B). These fringes appear bright probably because of lower U + Th content, and might represent narrow metamorphic recrystallisation or overgrowth. However, because they are all considerably narrower than the SHRIMP analytical spot, they could not be dated. Three analyses were undertaken on sites where the oscillatory zoning internal to the grains appeared least recrystallised in the CL images (Fig. 5B). These oscillatory-zoned sites have high U abundance of ≥697 p.p.m., with high Th/U ratios ≥0.79. The high Th/U is typical for igneous zircon crystallised from mafic-intermediate magmas (Paces and Miller, 1993). All sites contain very small amounts of common Pb, and yield indistinguishable concordant albeit imprecise ages (Fig. 7A), with a weighted mean $^{206}Pb/^{238}U$ age of 448±35 Ma (95% confidence, MSWD=0.16, no rejects). The poor precision on the weighted mean is because of the few analyses used in this determination. 448 Ma is interpreted as the time of magmatic crystallisation of the gabbroic protolith of the amphibolite (Upper Ordovician – Katian).

Sample 417 is from a massive mafic pluton southeast of Meydanak village (Fig. 4), which was mapped by Mohajjel (1997) as intrusive into Permian metacarbonate rocks and cross-cutting units of the June Complex. In contrast, the Shazand 1:100,000 geological map shows this pluton entirely within the June Complex and not in contact with the Permian metacarbonate unit (Sahandi et al., 2006). Although this pluton was not dated by Shakerardakani et al. (2015), they considered that it was most likely Middle Jurassic on basis of a LA-ICP-MS U/Pb zircon age of 170±3 Ma from an inferred equivalent gabbro in a sill south of the Kuh-e-June Metacarbonate (sample T-108, Fig. 4). Gabbro sample 417 yielded abundant large euhedral prismatic zircons, which had commonly fragmented during mineral separation in the laboratory. All grains show well-developed micron-scale igneous oscillatory zoning, parallel to preserved euhedral grain boundaries (Fig. 5C). The oscillatory zoned zircon has high U abundance of ≥749 p.p.m., with high Th/U ratios mostly ≥1. The high Th/U is typical for igneous zircon crystallised from mafic-intermediate magmas (Paces and Miller, 1993). All sites contain very small amounts of common Pb, and yield indistinguishable concordant ages (Fig. 7B), with a weighted mean $^{206}Pb/^{238}U$ age of 336±9 Ma (95% confidence, MSWD=0.04, no rejects). This is interpreted as the time of magmatic crystallisation of the gabbro (Carboniferous – Visean). This age is slightly older than the age of 315±4 Ma

determined by Shakerardakani et al. (2015) for a metagabbro east-northeast of Meydanak village (Fig. 4).

Three samples were collected and pooled from andalusite-garnet-biotite schist in the Hamadan Phyllite at a locality 35 km southeast of Hamadan (Fig. 3, sample HS). The sample gave a low yield of small zircons. Most grains are prisms or fragments of prisms, typically 150-50 µm long. In CL images the grains are dominated by igneous-style oscillatory zoning, but overprinted by recrystallisation domains. However, unlike the zircons in amphibolite sample 813, the HS zircons do not have CL-bright micron-scale low U + Th selvedges (Fig. 5D). Six analyses were undertaken on better-preserved oscillatory-zoned domains in 5 grains. U contents are >549 p.p.m. with all Th/U ratios >0.12 and up to 1.01. All grains yielded U-Pb ages indistinguishable from Concordia (Fig. 7C). Four grains, including the one with duplicate analyses yielded Palaeozoic ages, whereas the fifth (grain #4) yielded a Late Palaeoproterozoic age. Two analyses on a long aspect ratio prism yielded indistinguishable ages, with a weighted mean $^{206}Pb/^{238}U$ age of 270±12 Ma (95% confidence, MSWD=0.02). Analysis of grain #3 yielded a somewhat younger $^{206}Pb/^{238}U$ age than the grain #1 analyses. However, this site appears darker and more crystallised in the CL image, and the measured content of common Pb is higher (f^{206}(%) = 0.063; Table 1). Therefore it could be isotopically disturbed and not considered further. Consequently the 270 Ma age for grain #1 is interpreted as the youngest detrital component in this sample, and gives the maximum time of deposition as Middle Permian (Roadian).

4.2 Lu-Hf isotopes

Fourteen Lu-Hf isotopic determinations were undertaken on 14 zircons from gabbro sample 417, with five of these sites (7.1 to 11.1) overlain onto the previous SHRIMP U-Pb craters (Table 2). Using the zircon U-Pb crystallisation age of 336 Ma, the initial ε_{Hf} values range, from +3.8 to +8.3, with T_{DM} (depleted mantle) model ages ranging from 620 to 820 Ma (Table 2; Fig. 8). These data show spread of initial ε_{Hf} values beyond analytical error, and significantly older (Neoproterozoic) T_{DM} model ages than the age of igneous crystallisation. We suggest that this indicates small and variable amounts of contamination of the mantle-derived gabbroic magma by Precambrian Sanandaj-Sirjan Zone basement. The plausibility of this is shown by the gabbro zircon initial Hf data plotting between DM and Neoproterozoic crust (ε_{Hf} <-2.7) of the Sanandaj-Sirjan Zone at 336 Ma (Fig. 8; data from Nutman et al., 2014).

5. Discussion

5.1 Pan-African basement

Pan-African basement has been determined from U-Pb zircon ages on granitic and metamorphic rocks in the northwest Sanandaj-Sirjan Zone from east of Golpaygan as well as the Galeh-Doz Orthogneiss (Hassanzadeh et al., 2008; Nutman et al., 2014; Shakerardakani et al., 2015). Plutonic rocks from farther to the northwest in the Sanandaj-Sirjan Zone, around Lake Urumieh also have Pan-African zircon ages (Hassanzadeh et al., 2008; Moghadam et al., 2015). These occurrences are consistent with the Sanandaj-Sirjan Zone having a Pan-African basement similar to that found in the Zanjan region of northwest Iran and elsewhere in Central Iran such as in the Yazd Block and in northern Central Iran (Figs. 2, 8) (Ramezani and Tucker,

2003; Verdel et al., 2007; Hassanzadeh et al., 2008; Saki, 2010a, b; Rahmati-Ilkhchiet al., 2011; Balaghi Einalou et al., 2014). Pan-African basement ages are common in the Cimmerian continental fragment in central and northern Iran but have not been identified as a basement component of the Turan Platform (Şengör and Natal'lin, 1995; Natal'in and Şengör, 2005).

The Pan-African granites and metamorphic rocks of northern Central Iran show rapid orogenic development at 550 to 540 Ma involving sedimentation, deformation, metamorphism and arc plutonism with generation of abundant S-type granites by anataxis and are thought to occur along an extension of the north-facing Cadomian magmatic arc at the northern margin of Gondwana, although probably separated from it by a backarc basin (Kounov et al., 2012; Balaghi Einalou et al., 2014). The Galeh-Doz Orthogneiss is an A-type pluton and has been interpreted as emplaced in an extensional post-collisional setting (Shabanian et al., 2009) consistent with an inferred backarc setting southwest of the Cadomian arc in Central Iran. Counter-clockwise block rotations in Central Iran in the Late Jurassic and Neogene (Matteii et al., 2012, 2015) do not significantly affect this arrangement assuming that the Sanandaj-Sirjan Zone was a coherent elongate assemblage in the early Mesozoic and Palaeozoic.

Zircons in the Carboniferous gabbro with a U-Pb zircon age of 336 Ma have initial ε_{Hf} values of +4 to +8 compatible with contamination by Neoproterozoic crust of a gabbroic magma derived from the depleted mantle. Thus the Carboniferous continental crust of the Sanandaj-Sirjan Zone had a significant Neoproterozoic component consistent with its derivation from northern Gondwana where Neoproterozoic Pan-African crustal development was widespread (Stern, 2002). This further supports the Gondwanan origin of the Sanandaj-Sirjan Zone consistent with its Palaeozoic lithostratigraphy (Berberian and King, 1981) and contrary to the suggestion of Bea et al. (2011) that it was of Eurasian lineage.

5.2 Age of the June Complex

It is clear from the range of U-Pb zircon ages (Table 3) that the June Complex has a complicated history and included within it are rocks of Late Neoproterozoic to Triassic age. The relationship between the June Complex and the Late Neoproterozoic Galeh-Doz Orthogneiss is obscured due to strong overprinting by intense deformation (Mohajjel and Fergusson, 2000). An intrusive contact has not been conclusively identified and no contact metamorphic aureole in the June Complex has been found adjacent to the Galeh-Doz Orthogneiss (Shabanian et al., 2009). Given that the maximum depositional age of P17 quartzite from two detrital zircons is 547±32 Ma and this overlaps with the age of the Galeh-Doz Orthogneiss at 568±11 Ma (Nutman et al., 2014), the protolith granite could have been either intrusive into part of the June Complex or it has formed a basement upon which the quartzite, and potentially some of the carbonate and shaly succession of the protolith of the June Complex, was deposited.

Amphibolite and metagabbro in the June Complex have Ordovician and Carboniferous protolith ages and Middle Jurassic gabbro is intrusive into the June Complex (Table 3). Dolomite within regional equivalents of the June Complex contains localities with Triassic ages (Shakerardakani et al., 2015) but most of the June Complex carbonate rocks and schist lack fossils. The large mass of the Permian Kuh-e-June Metacarbonate adjacent to the June Complex (Fig. 4) is

puzzling, and presumably reflects thrust imbrication of disparate units as ages from the June Complex indicate Neoproterozoic-Cambrian, Ordovician and Triassic rocks, but no Permian rocks have been found within it. The relationship between the gabbro mass 5 km southeast of Meydanak village and the Permian Kuh-e-June Metacarbonate is unknown; previously it was regarded as intrusive but its older age rules this out. This gabbro is massive and lacks evidence for pervasive deformation but has only undergone low-temperature alteration (Shakerardakani et al., 2015).

Relationships cannot be inferred on the basis of the deformation in plutonic rocks – smaller bands of gabbro within the June Complex, such gabbro sample S-100 of Shakerardakani et al. (2015), have low-temperature alteration and are weakly deformed. In contrast, the gabbro mass 5 km southeast of Meyandak village is undeformed (Shakerardakani et al., 2015). This pluton was considered a late, post-tectonic mass of probable Cenozoic age on the basis of its undeformed state (Mohajjel, 1997; Mohajjel and Fergusson, 2000), but now our zircon age shows it is comparable in age to weakly deformed gabbro in the June Complex (Shakerardakani et al., 2015).

5.3 Carboniferous-Permian igneous rocks and rifting in the Sanandaj-Sirjan Zone

For the Iranian sector of Neo-Tethys, the consensus is that it formed by rifting in the Permian to Triassic (Berberian and King, 1981; Ricou, 1994; Alavi, 1994, 2004; Stampfli and Borel, 2002; Mohajjel et al., 2003; Agard et al., 2011; Mohajjel and Fergusson, 2014; Hassanzadeh and Wernicke, 2016). In neighbouring Oman, rifting and translation of Cimmeria away from the northern Gondwana margin occurred in the late Middle Permian (Chauvet et al., 2009). In the Sanandaj-Sirjan Zone, the Carboniferous to Permian plutonic rocks with an A-type and rift-related geochemical affinity indicate a long episode of igneous activity (335-285 Ma) associated with rifting from Gondwana in the initiation of Neo-Tethys (Fig. 9). The Carboniferous gabbroic rocks in the June Complex (Shakerardakani et al., 2015), the Late Carboniferous granites and gabbronorites along the northwest shore of Lake Urumieh (Moghadam et al., 2015), the Early Permian Hasanrobat Granite near Golypagan (Alirezaei and Hassanzadeh, 2012), have all been considered related to Permian opening of Neo-Tethys. In contrast, the Late Carboniferous A-type Khalifan Granite, south of Lake Urumieh, was considered by Bea et al. (2011) part of a Variscan event. We interpret the Khalifan Granite as part of the rift-related igneous activity associated with separation of Cimmeria from the northern margin of Gondwana because: (a) the timing of these plutonic rocks is consistent with rifting of Cimmeria from the northern margin of Gondwana (Fig. 9), and (b) these plutonic rocks have an A-type geochemical affinity consistent with rifting.

The Sanandaj-Sirjan Zone was rifted away from the northern margin of Gondwana and formed a ribbon microcontinent within Tethys (Şengör, 1984; Ricou, 1994; Stampfli and Borel, 2002). Rifting was associated with igneous activity from the Early Carboniferous onwards and although the timing of seafloor spreading and continental separation is constrained to the Late Permian in Oman (Chauvet et al., 2009), timing is less certain farther north in western Iran (Mohajjel and Fergusson, 2014). Timing of rifting in the Sanandaj-Sirjan Zone is only loosely constrained from the stratigraphic record. Deep-marine radiolarites, exposed adjacent to the Main Zagros Thrust, are indicative of a developing ocean basin no older than Early Jurassic (Gharib and De Wever, 2010; Mohajjel and Fergusson, 2014). The Bisotun limestones are also exposed near the Main Zagros Thrust and are Late Triassic to

the Middle-Late Cretaceous (Braud, 1978), and are interpreted as part of an outer microcontinental ribbon in Neo-Tethys neighbouring Gondwana (Kazmin et al., 1986). Thus for the Sanandaj-Sirjan Zone, separation of Cimmeria must have occurred by the Middle Triassic, but we favour Late Permian rifting, comparable with that in Oman (Chauvet et al., 2009), given the nearly 50 million year interval of igneous activity (336-288 Ma) that is documented in the Sanandaj-Sirjan Zone (Fig. 9).

5.4 Cimmerian Orogeny

From review of published K/Ar, Ar/Ar, Rb/Sr and U/Pb ages, and also considering unpublished data, Shakerardakani et al. (2015) concluded that metamorphism in the Sanandaj-Sirjan Zone was poly-phase with one event at ~180 Ma and a second metamorphic episode within 120-65 Ma. In the Hamadan region, the Hamadan Phyllite locally contains fossils as young as early Middle Jurassic (Baharifar et al., 2004) whereas our rare detrital zircons from the phyllite show that our sample is no older than the mid Permian. Additionally, plutonic rocks in the Hamadan region are typically massive and have contact metamorphosed the Hamadan Phyllite and are mid Jurassic (167-153 Ma; Ahmadi Khalaji et al., 2007; Shahbazi et al., 2010; Mahmoudi et al., 2011; Mohajjel and Fergusson, 2014). Therefore, we regard the greenschist to amphibolite facies metamorphism of the Hamadan Phyllite as mid Jurassic (~168-175 Ma), and immediately predating the mid Jurassic plutonic rocks in the Golpaygan-Hamadan region. This timing is marginally younger than the ~180 Ma metamorphic event recognised by Shakerardakani et al. (2015). The mid Jurassic orogenesis in the northwest Sanandaj-Sirjan Zone has been related to the late Cimmerian Orogeny in central Iran (Shakerardakani et al., 2015).

In northern Iran, unconformities associated with the Upper Triassic to Middle Jurassic Shemshak Group signify uplift generated by the continental collision that closed Paleo-Tethys (Wilmsen et al., 2009). A basal unconformity on the underlying plate was produced by uplift of the peripheral bulge near the Middle to Late Triassic boundary, and the main Early Jurassic Cimmerian unconformity, within the Shemshak Group, formed from uplift and deformation accompanying slab break-off in the collision and was followed by mid Jurassic subsidence (Wilmsen et al., 2009). Cimmerian deformation in the Alborz and Kopet Dagh is related to closure of Palaeo-Tethys, however evidence of late Cimmerian multiple deformation and metamorphism in the Hamadan-Golpayagan region (Mohajjel et al., 2003; Mohajjel and Fergusson, 2014), and early Cimmerian deformation and metamorphism in the southeast Sanandaj-Sirjan Zone around Sirjan (Sheikholeslami et al., 2008; Sheikholeslami 2015), are anomalous. We consider it unlikely that the Sanandaj-Sirjan Zone was once part of the Palaeo-Tethyan suture as it lacks the sedimentological evidence for continental collision found in northern Iran (Wilmsen et al., 2009) and has a Pan-African basement. Development of mid Jurassic metamorphic complexes in the Sanandaj-Sirjan Zone, in contrast to the widespread weakly metamorphosed Palaeozoic platformal-type successions in Central Iran (Berberian and King, 1981; Wendt et al., 2005) and the Zagros Fold and Thrust Belt (Alavi, 2004) indicate that the Sanandaj-Sirjan Zone is distinct.

Why does the Sanandaj-Sirjan Zone show evidence for Cimmerian orogenesis? How were metamorphic complexes such as the June Complex and the widespread Hamadan Phyllite generated? Our suggestion is that opening of extensional basins within continental fragments, such as in Iran and much more

widely documented in Turkey (Moix et al., 2008; Robertson et al., 2012), is more widespread than recognised. These extensional basins represent weak zones in the continental crust and were subsequently preferentially deformed during the rapidly changing tectonics as convergence was transferred from Paleo-Tethys to Neo-Tethys in the Triassic and Jurassic (Fig. 10). We suggest that opening of marginal oceanic basins has occurred within the Central Iran microcontinent, including the Sanandaj-Sirjan Zone, at various times including in the Jurassic for the Nain-Baft Ocean which was finally closed in the latest Cretaceous (Mendipour Ghazi et al., 2012; Mendipour and Moazzen, 2015). The June Complex and Hamadan Phyllite contain relicts of marginal basin deposits reflecting rifting with crustal thinning of part of the Sanandaj-Sirjan Zone, probably in the Permian during continental rifting away from northern Gondwana. With closure of Palaeo-Tethys along the Alborz and Kopet Dagh, subduction was initiated in Neo-Tethys beginning in the Late Triassic in the southeast (Arvin et al., 2007) and younging farther to the northwest. We attribute intense deformation and metamorphism in the June Complex and Hamadan Phyllite to mid Jurassic convergence along the southwest margin of the Central Iranian microcontinent following subduction initiation but predating calc-alkaline plutonism associated with the maturing subduction zone. Thus the Cimmerian Orogeny in the southwestern margins of the Sanandaj-Sirjan Zone is a consequence of Palaeo-Tethyan closure. Did the extensional regime result in thinning of the microcontinent to the point where new oceanic crust developed? This cannot be answered because the age of eclogites in the Chadegan “complex” is yet to be established. The Triassic age suggested by Davoudian et al. (2006, 2008) would indicate formation of oceanic crust that was subducted along with extended continental margin rocks to form the eclogites that were subsequently exhumed.

The setting for the Cimmerian Orogeny in the northwest Sanandaj-Sirjan Zone is thus considered to reflect a developing active continental margin with deformation and uplift of greenschist-amphibolite facies metamorphic rocks from depths of 10-30 km (Mohajjel, 1997; Mohajjel and Fergusson, 2014). In active continental margins, metamorphism is classically recognised in paired metamorphic belts with the magmatic arc associated with high temperature – low pressure metamorphism (Brown, 2010). An example of metamorphic rocks emplaced in a magmatic arc setting are regional low-grade metamorphic rocks and higher grade rocks, such as the Darwin metamorphic complex, in the southern Andes (Hervé et al., 2008; Klepeis et al., 2010; Maloney et al., 2011). Emplacement of the Darwin metamorphic complex was caused by closure of a Late Jurassic, thermally weakened, extensional Rocas Verdes basin in the Cretaceous with development of widespread ductile deformation and associated thrusting (Klepeis et al., 2010). This model has similarities to our suggestions for the significance of the Cimmerian Orogeny in the northwestern Sanandaj-Sirjan Zone (see above).

Data from Central Iran, including radiometric ages and mapping of a Variscan suture in the Anarak-Jandaq block, indicate that this block may have been connected with the Palaeo-Tethyan suture in northeast Iran (Bagheri and Stampfli, 2008; Zanchi et al., 2009, 2015). Palaeomagnetic data from Central Iran indicate substantial counter-clockwise rotations of the Lut, Tabas and Yazd blocks in the Late Jurassic and Neogene (Mattei et al., 2012, 2015), and thus requires substantial changes to the Jurassic and older palaeogeography (Fig. 11). It has been argued that in spite of the platformal Palaeozoic succession indicative of stable tectonic conditions throughout much of Iran (Berberian and King, 1981; Wendt et al., 2005), blocks such as the Anarak-Jandaq block were derived from the Palaeo-Tethyan

suture and transported to their present settings by block rotations and strike-slip tectonics (Bagheri and Stampfli, 2008). The configuration of these blocks and the Sanandaj-Sirjan Zone in the Jurassic (Fig. 11) is presently poorly constrained.

5.5 Structural interpretation of the June Complex

The structural history of the June Complex needs to be reconsidered given the geochronology presented by Nutman et al. (2014), Shakerardakani et al. (2015) and herein in the context of Cimmerian orogenesis. Several U-Pb zircon ages on the Galeh-Doz Orthogneiss indicate that it is Pan-African and therefore not synchronous with the D_2 deformation as considered by Mohajjel and Fergusson (2000). We interpret that the D_1 and D_2 deformations formed in a continuum during regional deformation associated with closure of an extensional basin along the western side of the Sanandaj-Sirjan Zone. The differences in structural styles between the domains containing mylonitic rocks and domains containing schist-carbonate rocks are considered caused by deformation partitioning during dextral transpression associated with the Cimmerian regional deformation.

The Cenozoic continental collision has resulted in development of northeast-dipping thrusts with uplift of the June Complex over Jurassic-Cretaceous weakly metamorphosed units along the Main Zagros Thrust. To the southeast in the Azna region, Cenozoic thrust faults have transported parts of the June Complex at least 10 km to the southwest indicating reworking of the complex in the continental collision (Mohajjel and Fergusson, 2014, figs. 5, 6).

6. Conclusions

(1) Our new U-Pb zircon ages confirm earlier results that show the development of Pan-African basement, Carboniferous-Permian igneous activity and Cimmerian orogenesis within the Sanandaj-Sirjan Zone in western Iran. The age of the June Complex northwest of Azna is established with a range of latest Neoproterozoic to Triassic. Cimmerian metamorphism and deformation occurred in the early Middle Jurassic in the Hamadan Phyllite and June Complex with reworking of Pan-African basement. This orogenic episode was followed by development of the mid-Jurassic magmatic arc in the Sanandaj-Sirjan Zone that reflected subduction of Neo-Tethyan oceanic crust following closure of Palaeo-Tethys (Mahmoudi et al., 2011; Mohajjel and Fergusson, 2014).
(2) Our interpretation is that the Sanandaj-Sirjan Zone was rifted away from Gondwana in the Late Permian with formation of a backarc basin with an attenuated continental basement that resulted in sea-floor spreading in Neo-Tethys.
(3) During the closure of Palaeo-Tethys, the attenuated margin to Central Iran was inverted with metamorphism and dextrally transpressive deformation resulting in development of the June Complex and Hamadan Phyllite in the Jurassic part of the Cimmerian Orogeny.
(4) Thus in Iran the Cimmerian Orogeny reflects closure of Palaeo-Tethys in the Alborz, Kopet Dagh and Yazd Block and oblique shortening of extensional basins in the Sanandaj-Sirjan Zone during the initiation of subduction in Neo-Tethys.

Acknowledgements

This research was supported by the GeoQuEST Research Centre of the University of Wollongong. Shane Paxton at the Research School of Earth Sciences of the Australian National University is thanked for carefully undertaking the zircon separations and finding rare zircons in most samples.

References

Agard, P., Omrani, J., Jolivet, L., Mouthereau, F., 2005. Convergence history across Zagros (Iran): Constraints from collisional and earlier deformation. International Journal of Earth Sciences Geologische Rundschau 94, 401–419.

Agard P., Omrani J., Jolivet L., Whitechurch H., Vrielynck B., Spakman W., Monie P., Meyer B., Wortel R. 2011. Zagros Orogeny: A subduction-dominated process. Geological Magazine 148, 692–725.

Ahmadi Khalaji, A., Esmaeily, D., Valizadeh, M.V., Rahimpour-Bonab, H., 2007. Petrology and geochemistry of the granitoid complex of Boroujerd, Sanandaj-Sirjan Zone, Western Iran. Journal of Asian Earth Sciences 29, 859–877.

Alavi, M., 1994. Tectonics of the Zagros Orogenic belt of Iran: New data and interpretations. Tectonophysics 229, 211–238.

Alavi, M., 2004. Regional stratigraphy of the Zagros fold-thrust belt of Iran and its proforeland evolution. American Journal of Science 304, 1–20.

Alirezaei, S., and Hassanzadeh, J., 2012, Geochemistry and zircon geochronology of the Permian A-type Hasanrobat granite, Sanandaj–Sirjan belt: A new record of the Gondwana break-up in Iran. Lithos 151, 122–134.

Allen, M., Armstrong, H.A., 2008. Arabia–Eurasia collision and the forcing of mid-Cenozoic global cooling. Palaeogeography, Palaeoclimatology, Palaeoecology 265, 52–58.

Arvin,M., Pan, Y., Dargahi, S.,Malekzadeh, A., Babaei, A., 2007. Petrochemistry of the Siah– Kuh granitoid stock southwest of Kerman, Iran: implications for initiation of Neothetys subduction. Journal of Asian Earth Sciences 30, 824–834.

Bagheri, S., Stampfli, G.M., 2008. The Anarak, Jandaq and Posht-e-Badam Metamorphic Complexes in Central Iran: New geological data, relationships and tectonic implications: Tectonophysics 451, 123–155.

Baharifar, A., Moinevaziri, H., Bellon, H., Pique, A., 2004. The crystalline complexes of Hamadan (Sanandaj–Sirjan zone, western Iran): metasedimentary Mesozoic sequences affected by Late Cretaceous tectono-metamorphic and plutonic events. Comptes Rendus Geoscience 336, 1443–1452.

Balaghi Einalou, M., Sadeghian, M., Zhai M., Ghasemi, H., Mohajjel, M., 2014. Zircon U–Pb ages, Hf isotopes and geochemistry of the schists, gneisses and granites in Delbar Metamorphic-Igneous Complex, SE of Shahrood (Iran): Implications for Neoproterozoic geodynamic evolutions of Central Iran. Journal of Asian Earth Sciences 92, 92–124.

Bea, F., Mazhari, A., Montero, P., Amini, S., Ghalamghash, J., 2011. Zircon dating, Sr and Nd isotopes, and element geochemistry of the Khalifan pluton, NW Iran: Evidence for Variscan magmatism in a supposedly Cimmerian superterrane. Journal of Asian Earth Sciences 40, 172–179.

Berberian, M., King, G.C.P., 1981. Towards a paleogeography and tectonic evolution of Iran. Canadian Journal of Earth Sciences 18, 210–265.

Black, L.P., Kamo, S.L., Allen, C.M., Aleinikoff, J.M., Davis, D.W., Korsch, R.J., Foudoulis, C., 2003. TEMORA 1: A new zircon standard for Phanerozoic U-Pb

geochronology. Chemical Geology 200, 155–170. doi:10.1016/S0009-2541 (03)00165-7.
Bouvier, A., Vervoort, J.D., and Patchett, J., 2008. The Lu–Hf and Sm–Nd isotopic composition of CHUR: constraints from unequilibrated chondrites and implications for the bulk composition of the terrestrial planets. Earth and Planetary Sciences Letters 280, 285–295.
Braud, J., 1987. Paleogéographique, magmatique et structural de la region Kermanshah, Iran. Thèse de étate, Universié de Paris, Paris, 430 p.
Brown, M., 2010. Paired metamorphic belts revisited. Gondwana Research 18, 45-59.
Chauvet, F., Dumont, T., Basile, C., 2009. Structures and timing of Permian rifting in the central Oman Mountains (Saih Hatat). Tectonophysics 475, 563–574.
Chu, M.-F., Chun, S.-L., Song, B., Liu, D.-Y., O'Reilly, S.Y., Pearson, N.J., Ji, J., and Wen, D.-J., 2002. Zircon U-Pb and Hf isotope constraints on the Mesozoic tectonics and crustal evolution of southern Tibet. Geology 34, 745–748. doi: 10.1130/G22725.1.
Cumming, G.L., Richards, J.R., 1975. Ore lead ratios in a continuously changing Earth. Earth and Planetary Science Letters 28, 155–171. doi:10.1016/0012-821X(75)90223-X.
Davoudian, A.R., Khalili, M., Noorbehsht, I., Dachs, E., Genser, J., Shabanian, N., 2006. Geochemistry of metabasites in the north of the Shahrekord, Sanandaj-Sirjan Zone, Iran. Neues Jahrbuch für Mineralogie – Abhandlungen 182, 291–298.
Davoudian, A.R., Genser, J., Dachs, E., Shabanian, N., 2008. Petrology of eclogites from north of Shahrekord, Sanandaj-Sirjan Zone, Iran. Mineralogy and Petrology 92, 393–413. doi:10.1007/s00710-007-0204-6.
Gharib, F., De Wever, P., 2010. Mesozoic radiolarians from the Kermanshah Formation (Iran). Comptes Rendus Palevol 9, 209–219.
Hassanzadeh, J., Stockli, D.F., Horton, B.K., Axen, G.J., Stockli, L.D., Grove, M., Schmitt, A.K., Walker, J.D., 2008. U–Pb zircon geochronology of late Neoproterozoic–Early Cambrian granitoids in Iran: Implications for paleogeography, magmatism, and exhumation history of Iranian basement. Tectonophysics 451, 71–96.
Hassanzadeh, J., Wernicke, B., 2016. The Neotethyan Sanadaj-Sirjan zone of Iran as an archetype for passive margin-arc transitions. Tectonics, 35, 586-621, doi: 10.1002/2015TC003926.
Hervé, F., Calderón, M., Faúndez, V., 2008. The metamorphic complexes of the Patagonian and Fuegian Andes. Geologica Acta 6, 43-53.
Hessami, K., Koyi, H.A., Talbot, C.J., Tabasi, H., Shabanian, E., 2001. Progressive unconformities within an evolving foreland fold-thrust belt, Zagros Mountains. Journal of the Geological Society of London 158, 969–981.
Hiess, J., Bennett, V.C., Nutman, A.P., Williams, I.S., 2009. In situ U–Pb, O and Hf isotopic compositions of zircon and olivine from Eoarchaean rocks, West Greenland: New insights to making old crust. Geochimica et Cosmochimica Acta 73, 4489–4516. doi:10.1016/j.gca.2009.04.019.
Horton, B.K., Hassanzadeh, J., Stockli, D.F., Axen, G.J., Gillis, R.J., Guest, B., Amini, A., Fakhari, M.D., Zamanzadeh, S.M., Grove, M., 2008. Detrital zircon provenance of Neoproterozoic to Cenozoic deposits in Iran: Implications for chronostratigraphy and collisional tectonics. Tectonophysics 451, 97–122.
Kazmin, V.G., Ricou, L.F., Sbortshikov, I.M., 1986. Structure and evolution of the passive margin of the eastern Tethys. Tectonophysics 123, 153–179.

Klepeis, K., Betka, P., Clarke, G., Fanning, M., Hervé, F., Rojas, L., Mpodozis, C., Thomson, S., 2010. Continental underthrusting and obduction during the Cretaceous closure of the Rocas Verdes rift basin, Cordillera Darwin, Patagonian Andes. Tectonics 29, TC3014, doi:10.1029/2009TC002610.

Kounov, A., Graf, J., Quadt, A.V., Bernoulli, D., Burg, J.P., Seward, D., Ivanov, Z., Fanning, M., 2012. Evidence for a ‘‘Cadomian’’ ophiolite and magmatic-arc complex in SW Bulgaria. Precambrian Research 212–213, 275–295.

Ludwig, K.R., 2003. Isoplot 3.0: A geochronological toolkit for Microsof Excel. Berkeley Geochronological Center Special Publication 4. Berkeley Geochronological Center, Berkeley, California, 70 p.

Mahmoudi, S., Corfu, F., Masoudi, F., Mehrabi, B., Mohajjel, M., 2011. U–Pb dating and emplacement history of granitoid plutons in the northern Sanandaj–Sirjan Zone, Iran. Journal of Asian Earth Sciences 41, 238–249.

Maloney, K.T., Clarke, G.L., Klepeis, K.A., Fanning, C.M., Wang, W., 2011. Crustal growth during back-arc closure: Cretaceous exhumation history of Cordillera Darwin, southern Patagonia. Journal of Metamorphic Geology 29, 649–672.

Mattei, M., Cifelli, F., Muttoni, G., Zanchi, A., Berra, F., Mossavvari, F., Safar Ali, E., 2012. Neogene block-rotation in Central Iran: evidence from paleomagnetic data. Geological Society of America Bulletin 124, 943–956.

Mattei, M., Cifelli, F., Muttoni, G., Rashid, H., 2015. Post-Cimmerian (Jurassic–Cenozoic) paleogeography and vertical axis tectonic rotations of Central Iran and the Alborz Mountains. Journal of Asian Earth Sciences 102, 92–101.

McQuarrie, N., van Hinsbergen, D.J.J., 2013. Retrodeforming the Arabia-Eurasia collision zone: Age of collision versus magnitude of continental subduction. Geology 41, 315–318.

Mehdipour Ghazi, J., Moazzen, M., Rahgoshay, M., Moghadam, H.S., 2012. Geochemical characteristics of basaltic rocks from the Nain ophiolite (Central Iran); constraints on mantle wedge source evolution in an oceanic back arc basin and a geodynamical model. Tectonophysics 574–575, 92–104.

Mehdipour Ghazi, J., Moazzen, M., 2015. Geodynamic evolution of the Sanandaj-Sirjan Zone, Zagros Orogen, Iran. Turkish Journal of Earth Sciences 24, 513-528.

Moghadam, H.S., Li, X.-H., Ling, X.-X., Stern, R.J., Santos, J.F., Meinhold, G., Ghorbani, G., Shahabi, S., 2015. Petrogenesis and tectonic implications of Late Carboniferous A-type granites and gabbronorites in NW Iran: geochronological and geochemical constraints. Lithos 212–215, 266–279.

Moghadam, H., Stern, R.J., 2011. Geodynamic evolution of upper Cretaceous Zagros ophiolites: formation of oceanic lithosphere above a nascent subduction zone. Geological Magazine 148, 762–801.

Mohajjel, M., 1997. Structure and tectonic evolution of Palaeozoic–Mesozoic rocks, Sanandaj–Sirjan Zone, western Iran. PhD Thesis, University of Wollongong, Wollongong, Australia (unpublished), 226 p.

Mohajjel, M., Fergusson, C.L., 2000. Dextral transpression in Late Cretaceous continental collision, Sanandaj–Sirjan Zone, western Iran. Journal of Structural Geology 22, 1125–1139.

Mohajjel, M., Fergusson, C.L., Sahandi, M.R., 2003. Cretaceous-Tertiary convergence and continental collision, Sanandaj-Sirjan Zone, western Iran. Journal of Asian Earth Sciences 21, 397–412.

Mohajjel M., Fergusson, C.L., 2014. Jurassic to Cenozoic tectonics of the Zagros Orogen in northwestern Iran. International Geology Review 56, 263–287.

Moix, P., Beccaletto, L., Kozur, H.W., Hochard, C., Rosselet, F., Stampfli, G.M., 2008. A new classification of the Turkish terranes and sutures and its implication for the paleotectonic history of the region. Tectonophysics 451, 7–39.

Moosavi, E., Mohajjel, M., Rashidnejad-Omran, N., 2014. Systematic changes in orientation of linear mylonitic fabrics: an example of strain partitioning during transpressional deformation in north Golpaygan, Sanandaj–Sirjan zone, Iran. Journal of Asian Earth Sciences 94, 55–67.

Natal'in, B.A., Şengör, A.M.C., 2005. Late Palaeozoic to Triassic evolution of the Turan and Scythian platforms: The pre-history of the Palaeo-Tethyan closure. Tectonophysics 404, 175– 202.

Nutman, A.P., Mohajjel, M., Bennett, V.C., Fergusson, C.L., 2014. Gondwanan Eoarchean Neoproterozoic ancient crustal material in Iran and Turkey: zircon U Pb–Hf isotopic evidence. Canadian Journal of Earth Sciences 51, 272–285.

Paces, J.B., Miller, J.D., 1993. Precise U–Pb ages of Duluth Complex and related mafic intrusions, northeastern Minnesota: geochronological insights to physical, petrogenetic, paleomagnetic, and tectonomagmatic processes associated with the 1.1 Ga Midcontinent Rift System. Journal of Geophysical Research 98, 13997–14013.

Patchett, P.J., Kouvo, O., Hedge, C.E., Tatsumoto, M., 1981. Evolution of continental crust and mantle heterogeneity: evidence from Hf isotopes. Contributions to Mineralogy and Petrology 78, 279-297.

Rahmati-Ilkhchi, M., Faryad, S.W., Holub, F.V., Košler, J., Frank, W., 2011. Magmatic and metamorphic evolution of the Shotur Kuh Metamorphic Complex (Central Iran). International Journal of Earth Sciences 100, 45–62.

Ramezani, J., Tucker, R.D., 2003. The Saghand region, central Iran: U-Pb geochronology, petrogenesis and implications for Gondwana tectonics. American Journal of Science 303, 622–665.

Ricou, L.E., 1994. Tethys reconstructed: plates, continental fragments and their boundaries since 260 Ma. From Central America to South-eastern Asia. Geodynamica Acta 7, 169–218.

Robertson, A.H.F., Parlak, O., Ustaömer, T., 2012. Overview of the Palaeozoic–Neogene evolution of Neotethys in the Eastern Mediterranean region (southern Turkey, Cyprus, Syria). Petroleum Geoscience 18, 381–404.

Russell, W.A., Papanastassiou, D.A., and Tombrello, T.A. 1978. Ca isotope fractionation on the Earth and other solar system material. Geochimica et Cosmochimica Acta, 42: 1075–1090. doi:10.1016/0016-7037(78)90105-9.

Sahandi, M.R., Radfar, J., Hoseinidoust, J., Mohajjel, M., 2006. Geological Map of the Shazand 1:100,000 Quadrangle 5857. Geological Survey of Iran, Tehran, Iran.

Saki, A., 2010a. Proto-Tethyan remnants in northwest Iran: Geochemistry of the gneisses and metapelitic rocks. Gondwana Research 17, 704–714.

Saki, A., 2010b. Mineralogy, geochemistry and geodynamic setting of the granitoids from NW Iran. Geological Journal 45, 451–466.

Scherer, E., Munker, C., Mezger, K., 2001. Calibration of the lutetium–hafnium clock. Science 293, 683–687. doi:10.1126/science.1061372. PMID: 11474108.

Şengör, A.M.C., 1984. The Cimmeride orogenic system and tectonics of Eurasia. Geological Society of America, Special, Paper 195, 82 p.

Şengör, A.M.C., Natal'in, B.A., 1996. Palaeotectonics of Asia: fragments of a synthesis. In: Yin, A., Harrison, M. (Eds.), The Tectonic Evolution of Asia, Rubey Colloquium. Cambridge University Press, Cambridge, 486–640.

Shabanian, N., Khalili, M., Davoudian, A.R., Mohajjel, M., 2009. Petrography and geochemistry of mylonitic granite from Ghaleh-Dezh, NW Azna, Sanandaj-Sirjan Zone, Iran. Neues Jahrbuch für Mineralogie – Abhandlungen 185, 233–248.

Shahbazi, H., Siebel, W., Pourmoafee, M., Ghorbani, M., Sepahi, A.A., Shang, C.K., Vousoughi Abedini, M., 2010. Geochemistry and U–Pb zircon geochronology of the Alvand plutonic complex in Sanandaj–Sirjan Zone (Iran): New evidence for Jurassic magmatism. Journal of Asian Earth Sciences 39, 668–683.

Shakerardakani, F., Neubauer, F., Masoudi, F., Mehrabi, B., Liu, X., Dong, Y., Mohajjel, M., Monfaredi, B., Friedi, G., 2015. Panafrican basement and Mesozoic gabbro in the Zagros orogenic belt in the Dorud–Azna region (NW Iran): Laser-ablation ICP–MS zircon ages and geochemistry. Tectonophysics 647–648, 146–171.

Sheikholeslami, M.R., 2015. Deformations of Palaeozoic and Mesozoic rocks in southern Sirjan, Sanandaj–Sirjan Zone, Iran. Journal of Asian Earth Sciences 106, 130–149.

Sheikholeslami, M.R., Pique, A., Mobayen, P., Sabzehei, M., Bellon, H., Hashem Emami, M., 2008. Tectono-metamorphic evolution of the Neyriz metamorphic complex, Quri-Kor-e-Sefid area (Sanandaj–Sirjan Zone, SW Iran). Journal of Asian Earth Sciences 31, 504–521.

Söderlund, U., Patchett, P.J., Vervoort, J.D., Isachsen, C.E., 2004. The 176Lu decay constant determined by Lu–Hf and U–Pb isotope systematics of Precambrian mafic intrusions. Earth and Planetary Science Letters 219, 311–324.

Stampfli, G.M., Borel, G.D., 2002. A plate tectonic model for the Paleozoic and Mesozoic constrained by dynamic plate boundaries and restored synthetic oceanic isochrons. Earth and Planetary Science Letters 196, 17–33.

Stampfli, G.M., Kozur, H.W., 2006. Europe from the Variscan to the Alpine cycles. In: Gee, D.G., Stephenson, R.A. (Eds.), European Lithosphere Dynamics. Geological Society of London, Memoirs 32, pp. 57–82.

Stern, R.J., 2002. Crustal evolution in the East African Orogen: A neodymium isotopic perspective. Journal of African Earth Sciences 34, 109–117.Thirlwall, M.F., Anczkiewicz, R., 2004. Multidynamic isotope ratio analysis using MC–ICP–MS and the causes of secular drift in Hf, Nd and Pb isotope ratios. International Journal of Mass Spectrometry 235, 59–81. doi:10.1016/j.ijms.2004.04.002.

Verdel, C., Wernicke, B.P., Ramezani, J., Hassanzadeh, J., Renne, P.R., Spell, T.L., 2007. Geology and thermochronology of Tertiary Cordilleran-style metamorphic core complexes in the Saghand region of central Iran. Geological Society of America Bulletin 119, 961–977.

Verdel, C., Wernicke, B.P., Hassanzadeh, J., Guest, B., 2011. A Paleogene extensional flare-up in Iran. Tectonics 30, TC3008, 20 p. doi:10.1029/2010TC002809.

Vervoort, J.D., Patchett, P.J., Söderlund, U., Baker, M., 2004. Isotopic composition of Yb and the determination of Lu concentrations and Lu/Hf ratios by isotope dilution using MC-ICPMS. Geochemistry, Geophysics and Geosystems 5, Q11002. doi:10.1029/2004GC000721.

Wendt, J., Kaufmann, B., Belka, Z., Farsan, N., Bavandpur, A.K., 2005. Devonian/Lower Carbonifeous stratigraphy, facies patterns and palaeogeography of Iran Part II. Northern and Central Iran. Acta Geologica Polonica 55, 31–97.

Williams, I.S., 1998. U-Th-Pb geochronology by ion microprobe. In Applications of microanalytical techniques to understanding mineralizing processes. In: M.A.

McKibben, W.C.P. Shanks III and W.I. Ridley (Editors). Society of Economic Geology Short Course 7, pp. 1–35.
Wilmsen, M., Fürsich, F.T., Seyed-Emami, K., Majidifard, M.R., Taheri, J., 2009. The Cimmerian Orogeny in northern Iran: tectono-stratigraphic evidence from the foreland. Terra Nova 21, 211–218.
Woodhead, J., Hergt, J., 2005. A preliminary appraisal of seven natural zircon reference materials for in situ Hf isotope determination. Geostandards and Geoanalytical Research 29, 183–195. doi:10.1111/j.1751-908X.2005.tb00891.x.
Woodhead, J., Hergt, J., Shelley, M., Eggins, S., Kemp, R., 2004. Zircon Hf isotope analysis with an excimer laser, depth profiling, ablation of complex geometries, and concomitant age estimation. Chemical Geology 209, 121– 135.
Zanchi, A., Malaspina, N., Zanchetta, S., Berra, F., Benciolini, L., Bergomi, M., Cavallo, A., Javadi, H.R., Kouhpeyma, M., 2015. The Cimmerian accretionary wedge of Anarak, Central Iran. Journal of Asian Earth Sciences 102, 45–72.
Zanchi, A., Zanchetta, S., Garzanti, E., Balini, M., Berra, F., Mattei, M., Muttoni, G., 2009. The Cimmerian evolution of the Nakhlak-Anarak area, Central Iran, and its bearing for the reconstruction of the history of the Eurasian margin. In: Brunet, M.F., Wilmsen, M., Granath, J.W. (Eds.), South Caspian to Central Iran Basins. Geological Society of London Special Publications 312, pp. 261–286.

Figures

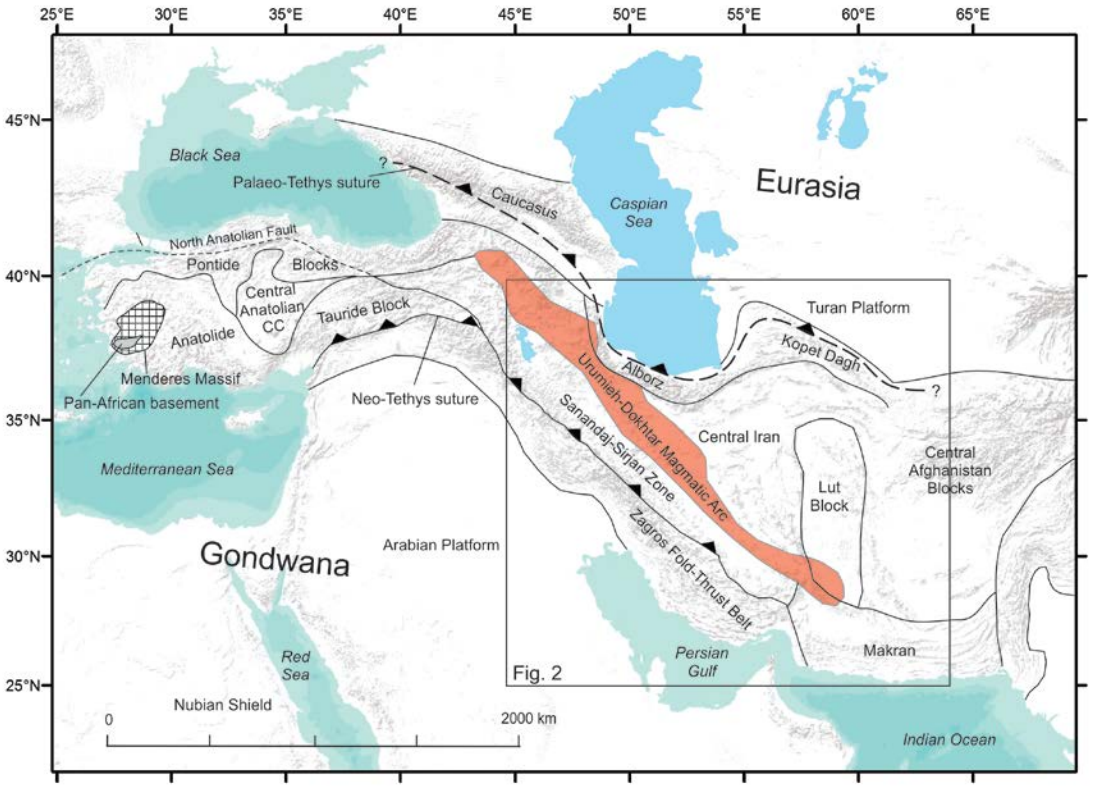

Fig. 1. Map showing the Palaeotethyan and Neotethyan sutures with the Cimmerian continent between Gondwana and Eurasia in the Middle East. Location of Fig. 2 indicated. Topography is from Environmental Systems Research Institute (ESRI,

Redlands, California) public domain data. Abbreviation: Central Anatolian CC—Central Anatolian Crystalline Complex.

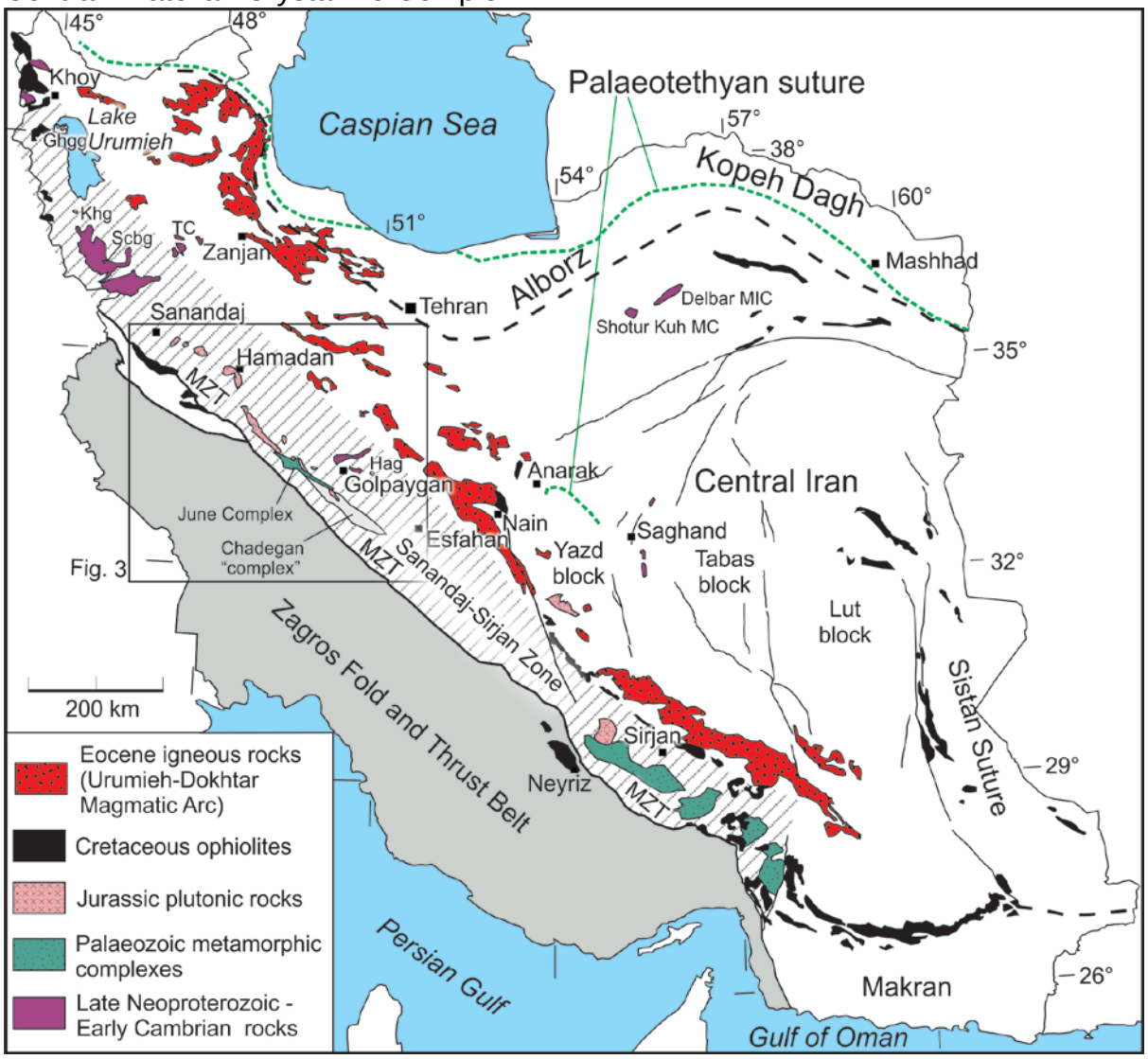

Fig. 2. Tectonic map of Iran including the Zagros Fold and Thrust Belt and the Sanandaj-Sirjan Zone that makes up the Zagros Orogen. Note the discontinuous Palaeotethyan suture in the Yazd Block well south of the Alborz and Kopeh Dagh (Bagheri and Stampfli, 2008). Pan-African igneous and metamorphic rocks include: the Takab Complex, Shotur Kuh Metamorphic Complex and the Delbar Metamorphic-Igneous Complex in the northern part of Central Iran, in the Yazd block near Saghand, the June Complex and other units around Golypagan, and the Sheikh Chupan-Bubaktan Granite northwest of Sanandaj (Verdel et al., 2007; Hassanzadeh et al., 2008; Saki, 2010a, b; Rahmati-Ilkhchi et al., 2011; Balaghi Einalou et al., 2014). In the Lake Urumieh region of the northwest Sanandaj-Sirjan Zone are Carboniferous plutons (Khalifan Granite, Bea et al., 2011; Ghushchi granites and gabbronorites, Moghadam et al., 2015) and a Permian pluton occurs east of Golpaygan (Hasanrobat Granite, Hag, Alirezaei and Hassanzadeh, 2012). Palaeozoic metamorphic rocks in the Sirjan and Neyriz region are from Sheikholeslami et al. (2008) and Sheikhaloslami (2015). Abbreviations: Delbar MIC—Delbar Metamorphic-Igneous Complex, Ghgg— Ghushchi granites and gabbronorites, Hag—Hasanrobat Granite, Khg— Khalifan Granite, MZT—Main Zagros Thrust, Scbg—Sheikh Chupan-Bubaktan Granite, TC—Takab Complex.

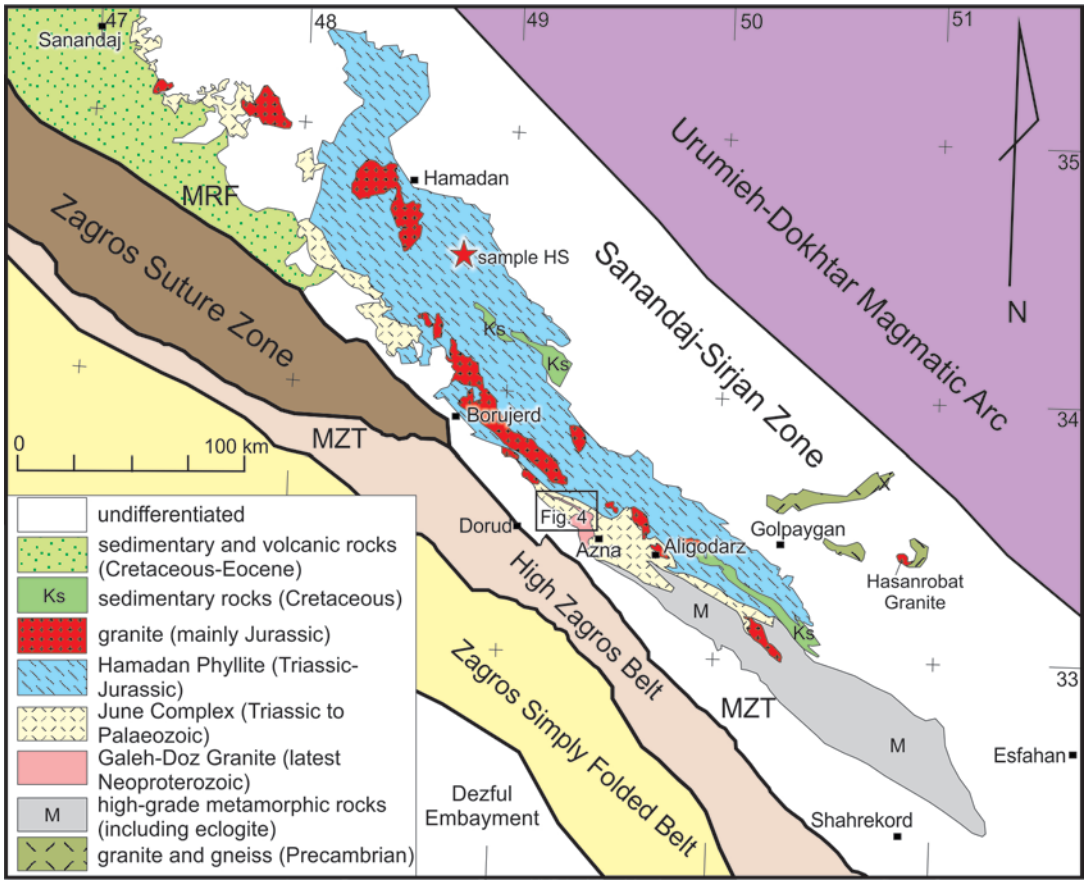

Fig. 3. Regional setting of the June area northwest of Azna and location of sample HS. Only selected units are shown for the Sanandaj-Sirjan Zone. Most of the undifferentiated area consists of Quaternary cover units and low-grade metamorphosed Cretaceous rocks. Abbreviations: MRF—Main Recent Fault, MZT—Main Zagros Thrust. See Fig. 1 for location.

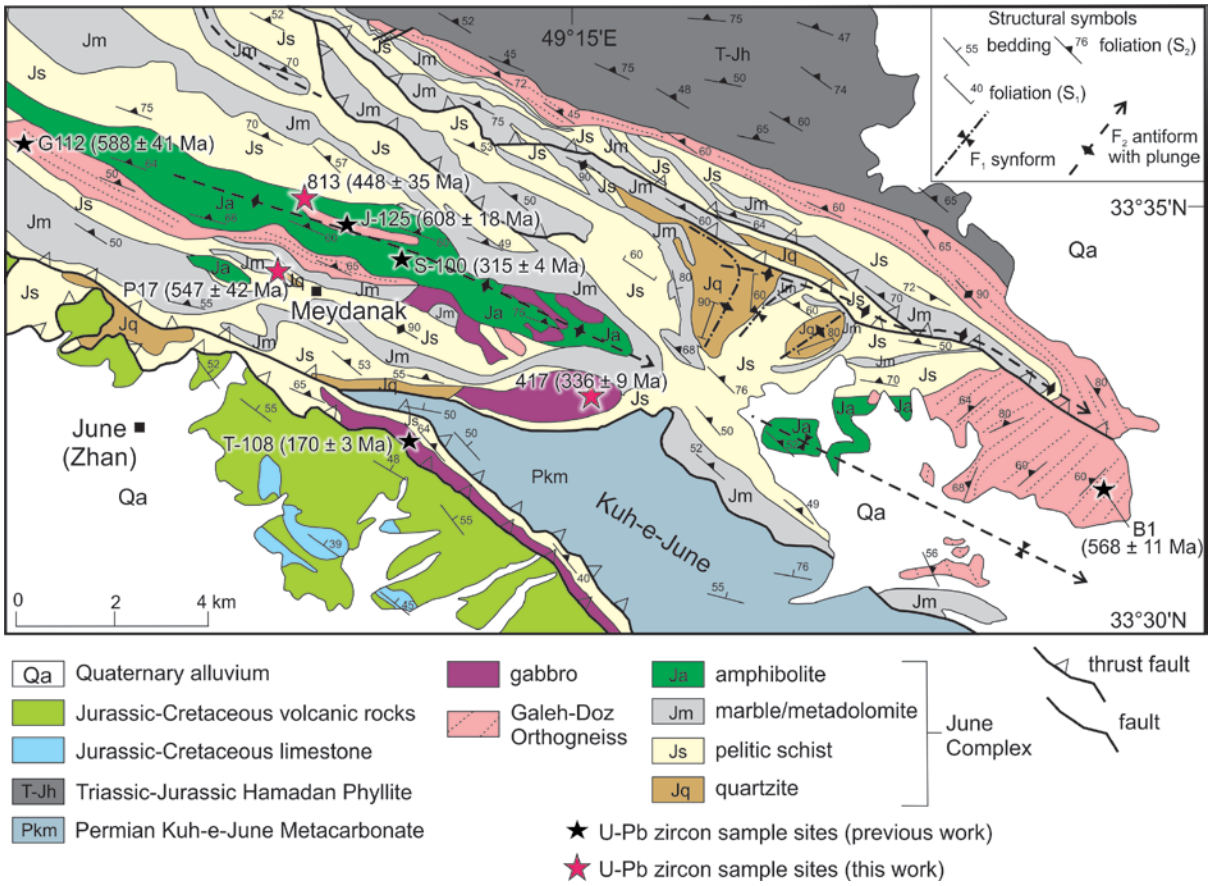

Fig. 4. Sample locations and geology of the June Complex in the June area northwest of Azna (redrawn and interpreted from Mohajjel, 1997; Mohajjel and Fergusson, 2000; Sahandi et al., 2006; Shakerardakani et al., 2015). Structural data from Mohajjel (1997) and Mohajjel and Fergusson (2000). Ages of the Galeh-Doz Orthogneiss from Nutman et al. (2014, sample B41) and Shakerardakani et al. (2015, samples J-125 and G112). Gabbro samples S-100 and T-108 are from Shakerardakani et al. (2015). See Fig. 3 for location. Samples P17, 813, and 417 are from this work. The Permian metacarbonate unit forms a prominent mountainous ridge with high points approaching 3000 m asl (Kuh-e-June). Note that June is also known as “Zhan”.

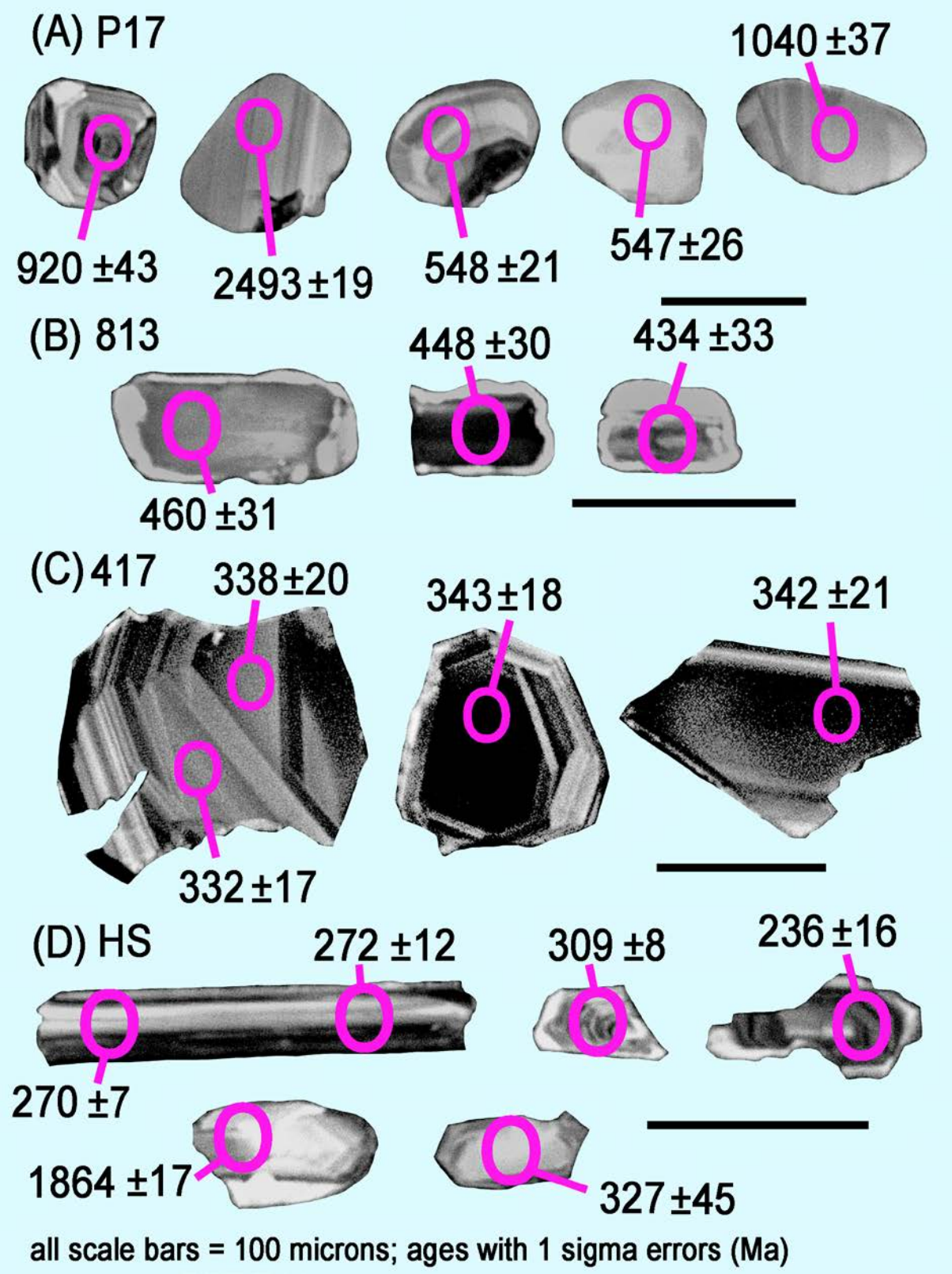

Fig. 5. Cathodoluminescence images of representative zircons. Ages (±σ) are given. All zircons are shown at the same scale. (A) Sample P17, quartzite from the June Complex, (B) sample 813, amphibolite from the June Complex, (C) sample 417, gabbro/diorite cross-cutting the June Complex, and (D) sample HS, schist from the Hamadan Phyllite.

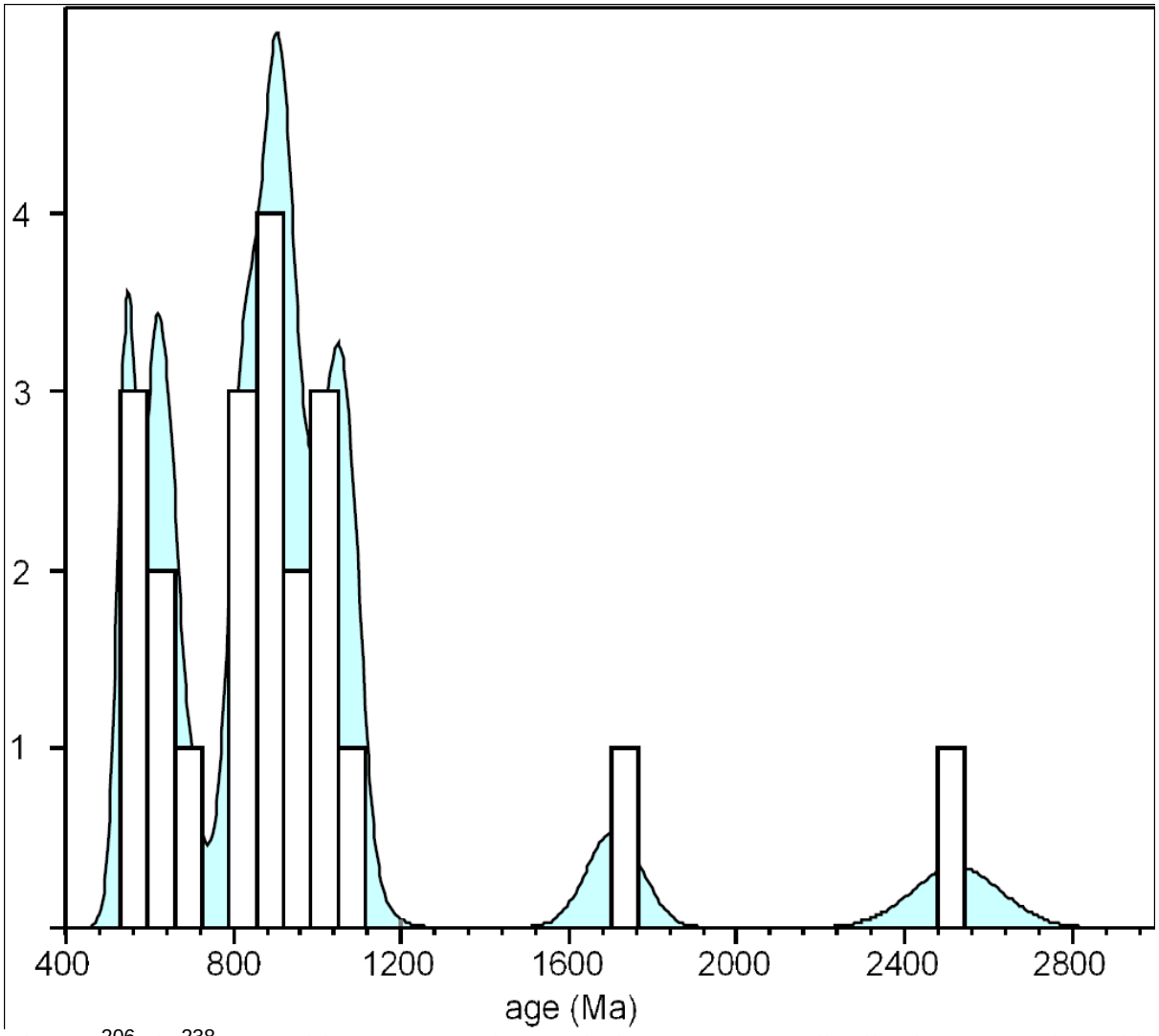

Fig. 6. $^{206}Pb/^{238}U$ age histogram and cumulative frequency distribution for grains with close to concordant ages from the quartzite sample P17.

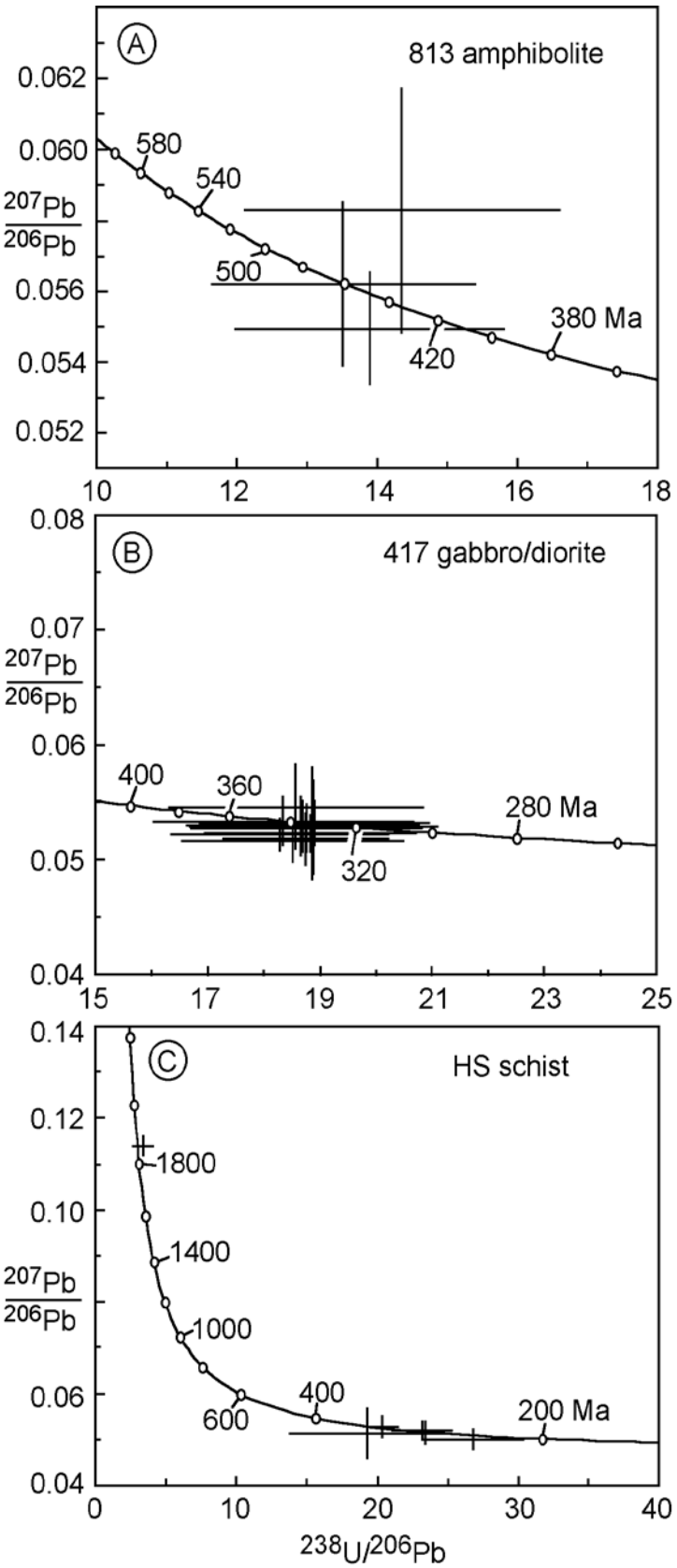

Fig. 7. (A) Tera–Wasserburg $^{238}U/^{206}Pb$ versus $^{207}Pb/^{206}Pb$ plot for amphibolite sample (813). (B) Tera–Wasserburg $^{238}U/^{206}Pb$ versus $^{207}Pb/^{206}Pb$ plots for gabbro sample 417. (C) Tera–Wasserburg $^{238}U/^{206}Pb$ versus $^{207}Pb/^{206}Pb$ plot for 3 samples of Hamadan Phyllite (HS1, HS2, HS3).

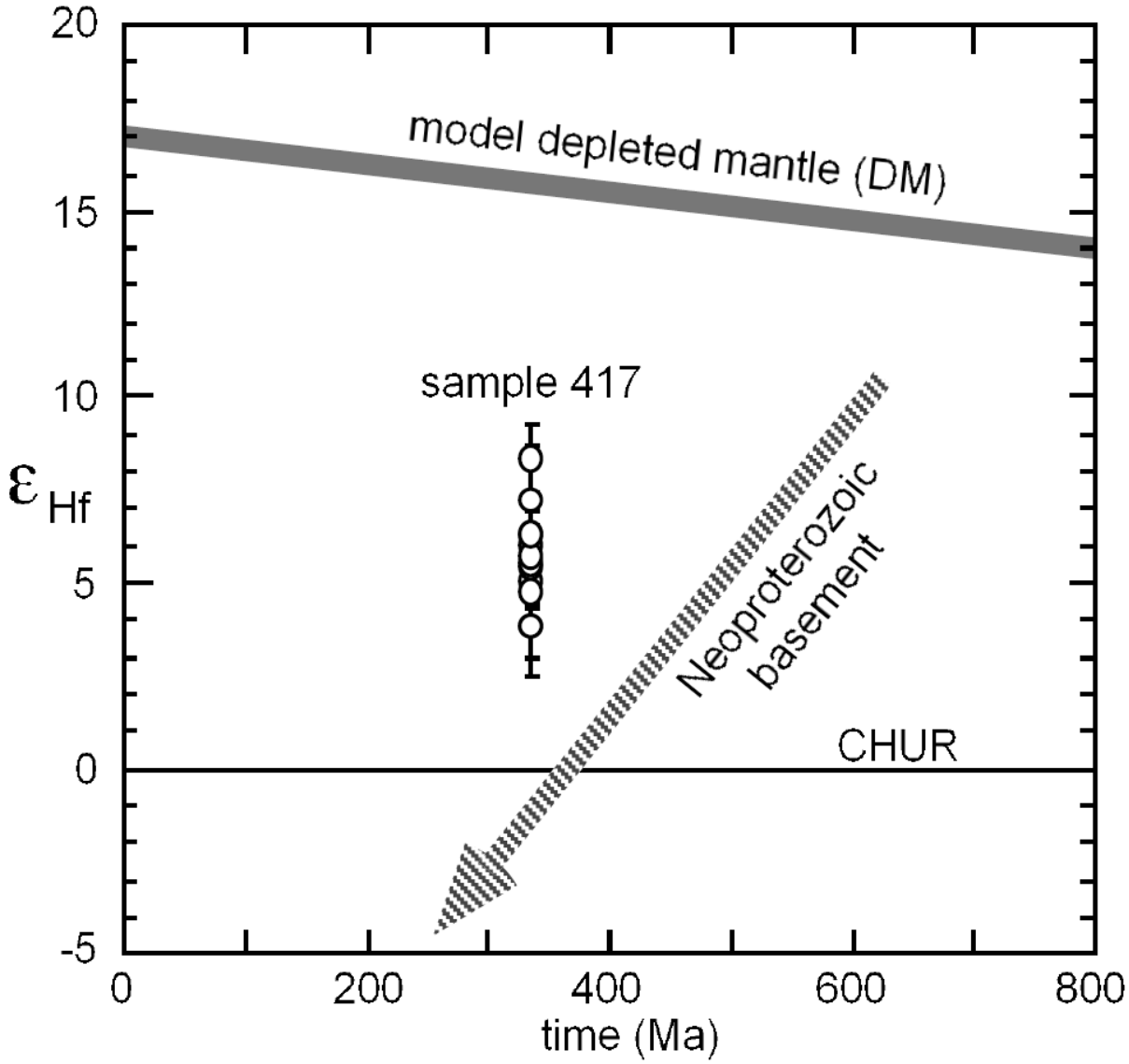

Fig. 8. Time – ε_{Hf} zircon plot for Carboniferous gabbro sample 417. The trajectory for Neoproterozoic basement uses data from Nutman et al. (2014).

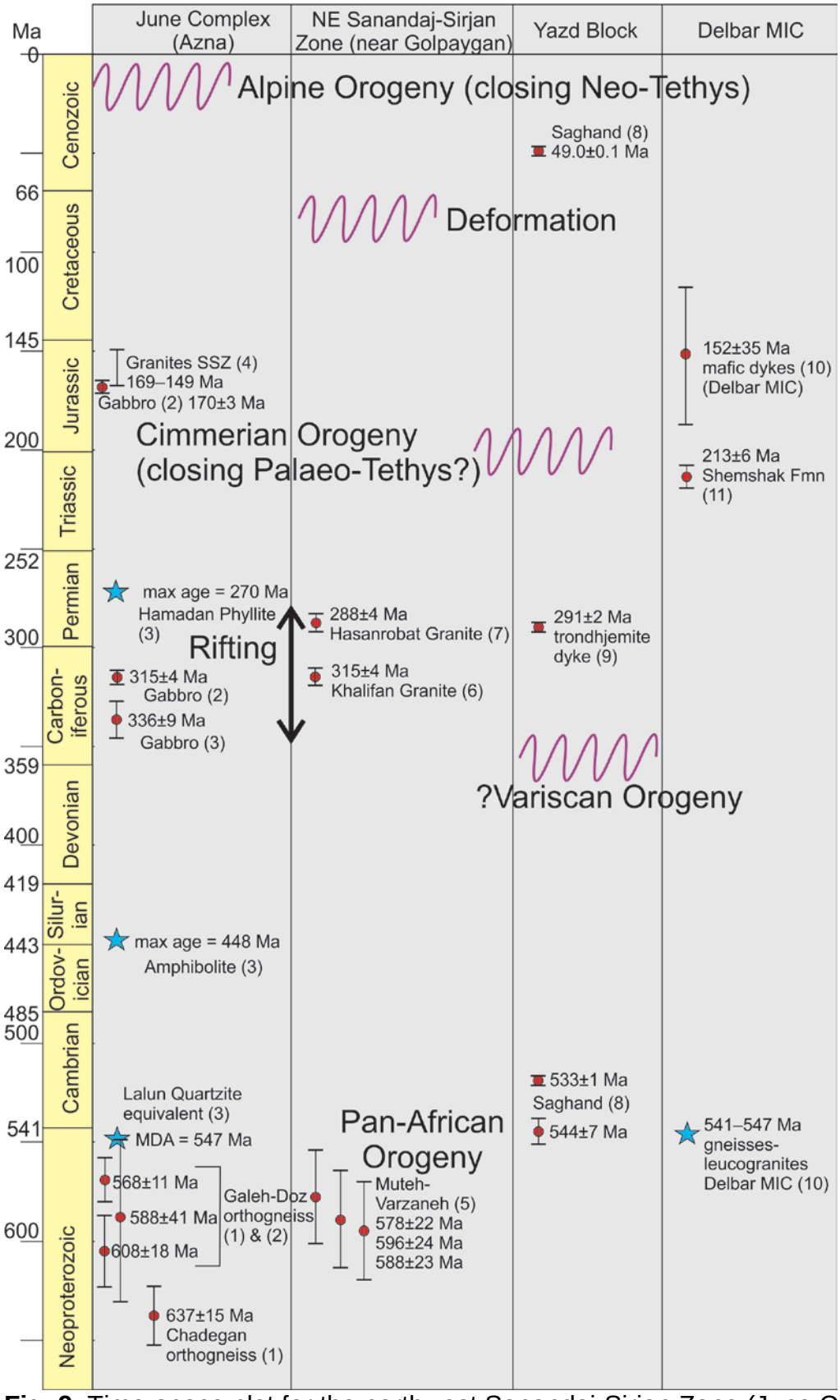

Fig. 9. Time-space plot for the northwest Sanandaj-Sirjan Zone (June Complex near Azna and northeast near Golpaygan and south of Lake Urumieh), the Yazd Block in Central Iran and the Delbar Metamorphic-Igneous Complex in northern Central Iran (see Fig. 2 for locations). References: (1) Nutman et al. (2014), (2) Shakerardakani

et al. (2015), (3) this work, (4) Mahmoudi et al. (2011), (5) Hassanzadeh et al. (2008), (6) Bea et al. (2011), (7) Alirezaei and Hassanzadeh (2012), (8) Ramezani and Tucker (2003), Verdel et al. (2007), (9) Zanchi et al. (2015) , (10) Balaghi Einalou et al. (2014), and (11) Horton et al. (2008).

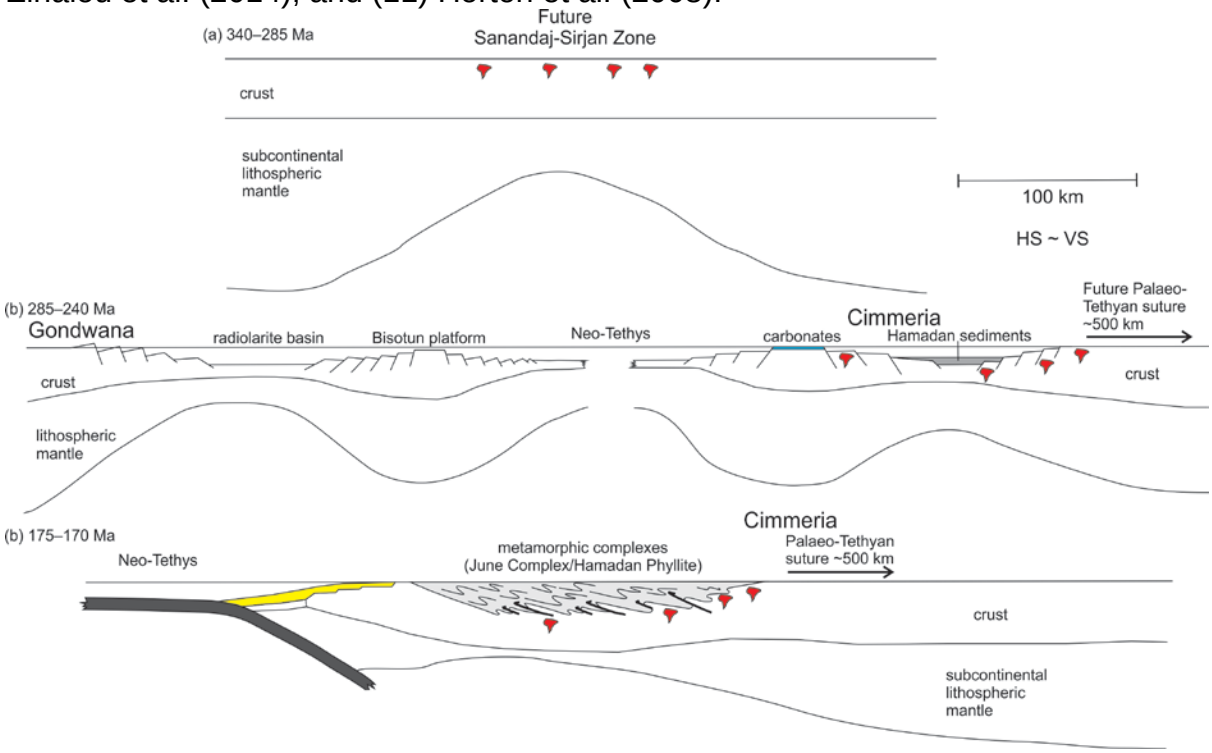

Fig. 10. Cross sectional models for the extensional basins formed in the Late Permian and deformed in the mid Jurassic in the northwest Sanandaj-Sirjan Zone.

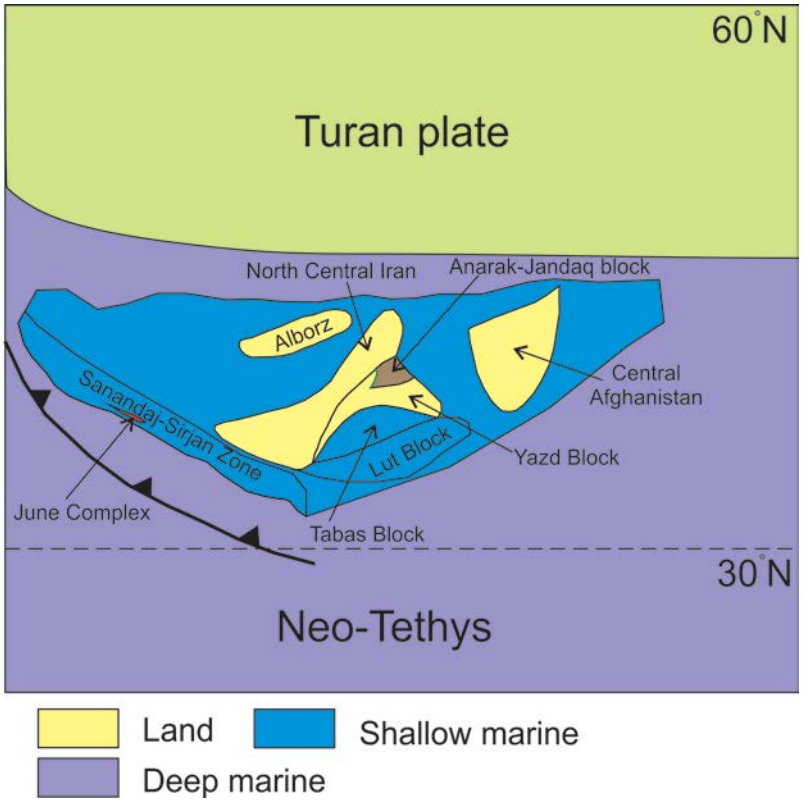

Fig. 11. Jurassic palaeogeography (~170 Ma) of Central Iran and the Sanandaj-Sirjan Zone showing the arrangement of various blocks prior to counter-clockwise

rotations in the Late Jurassic and Neogene (modified from Mattei et al., 2015). Note the Anarak-Jandaq block is part of the present-day Yazd Block and contains part of the Variscan suture. It is considered displaced from an original location in northeast Iran (Bagheri and Stampfli, 2008; Zanchi et al., 2015). The location of the Sanandaj-Sirjan Zone is consistent with it containing the magmatic arc along the southwestern margin of the Central Iranian blocks in the mid Jurassic (Mohajjel and Fergusson, 2014). The Turan plate is separated from Central Iran by deep marine of the Southern Caspian Basin.

Tables

Table 1. U-Pb zircon data for samples from the June Complex and Hamadan Phyllite, Sanandaj-Sirjan Zone, western Iran.

Table 1. U-Pb zircon data for samples from the June Complex and Hamadan Phyllite, Sanandaj-Sirjan Zone, western Iran.

Labels	site	U/ppm	Th/ppm	Th/U	f206%	$^{238}U/^{206}Pb$			$^{207}Pb/^{206}Pb$			age $^{206}Pb/^{238}U$			age $^{207}Pb/^{206}Pb$			%conc
417 gabbro																		
1.1	m,osc,p,fr	899	799	0.89	0.060	18.75	±	0.74	0.0518	±	0.0011	334.9	±	12.8				
2.1	m,osc,p,fr	910	440	0.48	0.037	18.58	±	1.13	0.0546	±	0.0018	338.0	±	20.1				
2.2	e,osc,p,fr	782	634	0.81	0.007	18.90	±	1.02	0.0532	±	0.0010	332.3	±	17.4				
3.1	e,osc,p,fr	1144	1128	0.99	0.032	18.83	±	0.94	0.0523	±	0.0008	333.5	±	16.3				
4.1	e,osc,p,fr	698	763	1.09	0.074	18.89	±	1.10	0.0529	±	0.0020	332.6	±	19.0				
5.1	m,osc,p,fr	1242	764	0.61	0.020	18.52	±	0.98	0.0516	±	0.0009	339.1	±	17.5				
6.1	e,osc,p,fr	882	2212	2.51	0.034	18.65	±	0.88	0.0529	±	0.0013	336.7	±	15.5				
7.1	e,osc,p,fr	749	768	1.03	0.056	18.77	±	1.03	0.0527	±	0.0010	334.6	±	17.9				
8.1	m,osc,p	2042	3768	1.84	0.018	18.29	±	0.97	0.0522	±	0.0007	343.3	±	17.8				
9.1	m,osc,p,fr	694	967	1.39	0.023	18.70	±	1.03	0.0530	±	0.0011	335.9	±	18.1				
10.1	e,osc,p	755	136	0.18	0.167	18.87	±	0.72	0.0532	±	0.0024	332.9	±	12.5				
11.1	e,osc/h,p,fr	1836	3388	1.85	0.026	18.35	±	1.15	0.0533	±	0.0011	342.2	±	21.0				
813 amphibolite																		
1.1	m,h/osc,p	697	847	1.22	0.009	13.52	±	0.94	0.05618	±	0.0012	460.1	±	30.91				
2.1	m,h,p,fr	1791	3276	1.83	0.005	13.89	±	0.95	0.05493	±	0.0008	448.1	±	29.78				
3.1	m,h/osc,p	1058	837	0.79	0.043	14.35	±	1.12	0.05826	±	0.0017	434.2	±	32.89				
HS schist																		
1.1	e,osc,p	1496	450	0.30	0.031	23.39	±	0.63	0.0516	±	0.0012	269.9	±	7.1				
1.2	e,osc,p	1441	564	0.39	0.038	23.22	±	1.06	0.0520	±	0.0009	271.9	±	12.1				
2.1	e,osc,p,fr	1236	1251	1.01	0.043	20.34	±	0.53	0.0528	±	0.0012	309.4	±	7.9				
3.1	e,osc,p,fr	1254	468	0.37	0.063	26.78	±	1.80	0.0501	±	0.0011	236.4	±	15.6				
4.1	m,osc,p	683	154	0.23	0.028	3.39	±	0.36	0.1140	±	0.0011	1666	±	157	1864	±	17	89
5.1	m,h,p	549	64	0.12	0.049	19.24	±	2.73	0.0514	±	0.0027	326.7	±	45.4				
P17 quartzite																		
1.1	m,osc,eq	818	437	0.53	0.009	6.52	±	0.32	0.0688	±	0.0007	920	±	43	894	±	23	103
2.1	m,h,p,fr	130	83	0.64	0.915	6.53	±	0.27	0.0741	±	0.0049	919	±	36	1045	±	139	88
3.1	m,osc,p	222	163	0.74	0.196	5.72	±	0.45	0.0741	±	0.0018	1038	±	75	1043	±	49	100
4.1	m,osc,rou	148	115	0.77	0.144	2.09	±	0.10	0.1636	±	0.0019	2525	±	105	2493	±	19	101
5.1	m,osc/h,p	1461	39	0.03	0.040	10.36	±	0.68	0.0572	±	0.0009	594.2	±	37.6				
6.1	e,osc,p	235	143	0.61	0.128	7.50	±	0.34	0.0645	±	0.0016	807	±	34	759	±	52	106
7.1	e,osc,rou	172	100	0.58	0.343	11.28	±	0.45	0.0565	±	0.0026	547.6	±	21.2				
8.1	m,osc,fr	387	237	0.61	0.046	3.29	±	0.14	0.0985	±	0.0061	1709	±	66	1596	±	120	107
9.1	e,osc,p	474	137	0.29	0.047	5.50	±	0.18	0.0742	±	0.0008	1077	±	33	1046	±	22	103
10.1	e,osc,p	475	114	0.24	0.104	6.71	±	0.25	0.0651	±	0.0021	896	±	31	777	±	71	115
11.1	m,h,p	152	67	0.44	0.125	6.66	±	0.35	0.0693	±	0.0017	902	±	44	908	±	51	99
12.1	e,h,rou	139	133	0.96	0.104	11.29	±	0.55	0.0575	±	0.0024	547.2	±	25.7				
13.1	e,osc,p	505	157	0.31	0.034	7.27	±	0.29	0.0644	±	0.0013	831	±	32	755	±	42	110
14.1	m,osc,rou	67	35	0.53	0.635	5.71	±	0.22	0.0716	±	0.0038	1040	±	37	975	±	113	107
15.1	m,osc,p,fr	301	78	0.26	0.086	5.66	±	0.24	0.0739	±	0.0016	1049	±	41	1038	±	45	101
16.1	m,h,rou	181	57	0.32	0.232	6.58	±	0.31	0.0684	±	0.0019	912	±	40	882	±	57	103
17.1	m,osc,rou	326	101	0.31	0.185	7.18	±	0.33	0.0661	±	0.0026	840	±	37	810	±	85	104
18.1	e,hd,p,fr	494	150	0.30	0.079	10.06	±	0.34	0.0604	±	0.0017	611.1	±	19.5				
19.1	m,osc,p	352	194	0.55	0.055	9.50	±	0.32	0.0614	±	0.0013	645.4	±	20.9				
20.1	e,osc,p	273	310	1.13	0.083	8.93	±	0.46	0.0626	±	0.0018	684.0	±	33.8				
21.1	m,osc,p	481	146	0.30	0.155	6.06	±	0.25	0.0710	±	0.0014	985	±	38	958	±	41	103
Site grain type and analysis location: p=prism, rou=rounded by abrasion, fr=fragment, e=end, m=middle																		
Site CL imagery: osc=oscillatory zoned, h=homogeneous, hd=homogeneous dark, low luminescence																		
All analytical errors are given a 1σ																		
Concordance and $^{207}Pb/^{206}Pb$ ages only given for >800 Ma old sites																		
f206% is the amount of ^{206}Pb modelled as non-radiogenic, based on measured ^{204}Pb																		

Table 2. Lutetium-Hafnium isotopic data, sample 417, Carboniferous gabbro.

Table 2. Lutetium-Hafnium isotopic data, sample 417, Carboniferous gabbro.

				Measured			$\varepsilon_{Hf}(0)$				initial		$T(DM)^1$
Analysis	$^{176}Lu/^{177}Hf$			$^{176}Hf/^{177}Hf$			in run errors (1SE)			U-Pb age (Ma)	$^{176}Hf/^{177}Hf$	$\varepsilon_{Hf}(t)$	(Ga)
1.1	0.000610	±	0.000008	0.282766	±	0.000013	-0.7	±	0.47	336	0.28276	6.7	0.68
2.1	0.000734	±	0.000016	0.282763	±	0.000011	-0.8	±	0.37	336	0.28276	6.5	0.69
3.1	0.000912	±	0.000023	0.282711	±	0.000017	-2.6	±	0.62	336	0.28270	4.6	0.77
4.1	0.000407	±	0.000002	0.282716	±	0.000010	-2.4	±	0.35	336	0.28271	5.0	0.75
5.1	0.000914	±	0.000026	0.282712	±	0.000012	-2.6	±	0.42	336	0.28271	4.7	0.76
6.1	0.001347	±	0.000002	0.282690	±	0.000012	-3.3	±	0.41	336	0.28268	3.8	0.80
7.1	0.000496	±	0.000006	0.282731	±	0.000022	-1.9	±	0.78	336	0.28273	5.4	0.73
8.1	0.001781	±	0.000056	0.282756	±	0.000020	-1.0	±	0.69	336	0.28274	6.0	0.72
9.1	0.001245	±	0.000081	0.282817	±	0.000014	1.1	±	0.50	336	0.28281	8.3	0.62
11.1	0.000766	±	0.000041	0.282749	±	0.000009	-1.3	±	0.30	336	0.28274	6.0	0.71
12.1	0.000400	±	0.000001	0.282746	±	0.000013	-1.4	±	0.45	336	0.28274	6.0	0.71
13.1	0.003011	±	0.000047	0.282797	±	0.000022	0.4	±	0.77	336	0.28278	7.2	0.68
14.1	0.002163	±	0.000013	0.282694	±	0.000019	-3.2	±	0.68	336	0.28268	3.8	0.82
15.1	0.000662	±	0.000004	0.282755	±	0.000009	-1.1	±	0.33	336	0.28275	6.3	0.70
16.1	0.000395	±	0.000003	0.282732	±	0.000015	-1.9	±	0.52	336	0.28273	5.5	0.73
17.1	0.000914	±	0.000001	0.282741	±	0.000009	-1.6	±	0.32	336	0.28273	5.7	0.72
18.1	0.001804		0.000065	0.282763		0.000016	-0.8		0.56	336	0.28275	6.3	0.71

[1] Depleted mantle (DM) model ages calculated using values for DM of $^{176}Hf/^{177}Hf=0.283251$ and $^{176}Lu/^{177}Hf=0.0384$

uncertainties are quoted at 1 sigma. Complete Hf isotopic compositions are given in Supplementary Data Table 2.

Table 3. Summary of U/Pb zircon ages from the June Complex and associated units north and east of June, Sanandaj-Sirjan Zone.

Table 3. Summary of U-Pb zircon ages from the June Complex and associated units north and east of June, Sanandaj-Sirjan Zone.

Unit	Lithology	Sample	Latitude	Longitude	Method	Age (Ma)	Reference
Galeh-Doz Orthogneiss	granitic gneiss	B1	33°31'37"N	49°23'16"E	SHRIMP	568 ± 11	Nutman et al. (2014)
Galeh-Doz Orthogneiss	granitic gneiss	G-112	33°36'41"N	49°06'26"E	LA-ICP-MS	588 ± 41	Shakerardakani et al. (2015)
Galeh-Doz Orthogneiss	granitic gneiss	J-125	33°35'38"N	49°23'16"E	LA-ICP-MS	608 ± 18	Shakerardakani et al. (2015)
June Complex	quartzite	P17	33°34'46.98"N	49°10'13.08"E	SHRIMP	547 ± 42	This work
Dare-Hedavand metagabbro	metagabbro (amphibolite facies)	S100	33°35'08"N	49°12'11"E	LA-ICP-MS	315 ± 4	Shakerardakani et al. (2015)
June Complex	amphibolite	813	33°35'38.83"N	49°10'54.42"E	SHRIMP	448 ± 35	This work
Darijune Gabbro	gabbro (epidote-amphibolite facies)	417	33°33'11.33"N	49°14'58.18"E	SHRIMP	336 ± 9	This work
Darijune Gabbro	gabbro (epidote-amphibolite facies)	T-108	33°32'40"N	49°12'19"E	LA-ICP-MS	170 ± 3	Shakerardakani et al. (2015)

Supplementary files

GoogleEarth, kmz file – June Complex and related samples, western Iran.

June Complex and related samples, western Iran.kmz

Supplementary Table 1. Standard Lu-Hf data summary (Australian National University Neptune 26-27 August 2015).

Supplementary Table 1. Standard Lu-Hf data summary (Australian National University Neptune 26-27 August 2015).

Analysis Name	$^{174}Hf/^{177}Hf$	1SE	$^{178}Hf/^{177}Hf$	1SE	$^{176}Lu/^{177}Hf$	1SE	$^{176}Hf/^{177}Hf$	1SE	**eHf(0)**	1SE
Plesovice-1	0.008662	0.000007	1.467336	0.000023	0.000090	0.000001	0.282481	0.000006	-10.76	0.23
Plesovice-2	0.008662	0.000009	1.467367	0.000023	0.000085	0.000001	0.282477	0.000009	-10.89	0.31
Plesovice-3	0.008641	0.000008	1.467358	0.000028	0.000101	0.000003	0.282476	0.000008	-10.92	0.29
Plesovice-4	0.008675	0.000008	1.467346	0.000025	0.000105	0.000001	0.282482	0.000009	-10.72	0.32
Plesovice-5	0.008661	0.000008	1.467388	0.000032	0.000102	0.000000	0.282482	0.000010	-10.73	0.36
Plesovice-6	0.008673	0.000008	1.467318	0.000030	0.000156	0.000001	0.282480	0.000007	-10.78	0.26
Plesovice-7	0.008656	0.000009	1.467390	0.000023	0.000117	0.000001	0.282474	0.000010	-11.00	0.35
Plesovice-8	0.008665	0.000008	1.467394	0.000022	0.000135	0.000000	0.282481	0.000008	-10.76	0.29
Average (this stud	*0.008662*				*0.000111*		*0.282479*	*±6 (2 SD)*	*-10.82*	
Accepted value (Slama et al., 2008)							***0.242482***	***±13 (2SD)***	***-10.82***	
MUDTANK-1	0.008651	0.000008	1.467374	0.000032	0.000031	0.000000	0.282540	0.000008	-8.66	0.29
MUDTANK-1	0.008671	0.000007	1.467329	0.000029	0.000019	0.000000	0.282507	0.000009	-9.85	0.33
MUDTANK-1	0.008654	0.000008	1.467336	0.000026	0.000005	0.000000	0.282518	0.000009	-9.45	0.32
MUDTANK-2	0.008666	0.000008	1.467355	0.000035	0.000022	0.000000	0.282520	0.000010	-9.38	0.35
MUDTANK-3	0.008654	0.000005	1.467303	0.000022	0.000018	0.000000	0.282486	0.000006	-10.57	0.23
MUDTANK-4	0.008662	0.000008	1.467351	0.000025	0.000022	0.000000	0.282526	0.000010	-9.17	0.35
MUDTANK-5	0.008677	0.000010	1.467329	0.000027	0.000029	0.000000	0.282521	0.000011	-9.34	0.38
MUDTANK-6	0.008678	0.000010	1.467341	0.000027	0.000016	0.000000	0.282519	0.000009	-9.40	0.31
MUDTANK-7	0.008668	0.000008	1.467362	0.000029	0.000005	0.000000	0.282515	0.000009	-9.56	0.30
MUDTANK-8	0.008661	0.000009	1.467326	0.000025	0.000016	0.000000	0.282508	0.000011	-9.81	0.38
Average (this stud	*0.008664*			*0.00003*	*0.000018*		*0.282516*	*±28 (2 SD)*	*-9.52*	*0.50*
Accepted value (Woodhead and Hergt, 2005)				***0.00004***			***0.282507***	***0.000006***	***-9.83***	***0.21***
QGNG-1	0.008656	0.000011	1.467383	0.000032	0.000878	0.000012	0.281621	0.000012	-41.18	0.43
QGNG-2	0.008674	0.000013	1.467349	0.000026	0.000943	0.000001	0.281611	0.000009	-41.51	0.33
QGNG-3	0.008650	0.000009	1.467374	0.000030	0.000710	0.000014	0.281599	0.000009	-41.95	0.31
QGNG-4	0.008675	0.000011	1.467408	0.000033	0.000473	0.000001	0.281624	0.000010	-41.05	0.36
QGNG-5	0.008655	0.000012	1.467372	0.000031	0.001009	0.000010	0.281614	0.000012	-41.41	0.41
QGNG-6	0.008659	0.000010	1.467365	0.000029	0.000919	0.000010	0.281623	0.000011	-41.09	0.38
QGNG-7	0.008649	0.000012	1.467404	0.000032	0.000591	0.000001	0.281627	0.000011	-40.95	0.40
QGNG-8	0.008669	0.000010	1.467411	0.000033	0.000464	0.000008	0.281612	0.000009	-41.49	0.32
QGNG-9	0.008651	0.000013	1.467348	0.000035	0.001273	0.000004	0.281631	0.000012	-40.82	0.43
Average (this stud	*0.0086597*		*1.467379*		*0.000807*		*0.281618*	*±20 (2 SD)*	*-41.27*	*0.35*
Accepted value (Woodhead and Hergt, 2005)					**0.000731**		**0.281612**	**0.000006**	**-41.50**	**0.21**
FC1-1	0.008661	0.000017	1.467372	0.000039	0.001324	0.000010	0.282186	0.000010	-21.18	0.35
FC1-2	0.008655	0.000010	1.467342	0.000029	0.001124	0.000017	0.282177	0.000009	-21.52	0.32
FC1-3	0.008658	0.000014	1.467428	0.000040	0.001256	0.000005	0.282194	0.000010	-20.90	0.37
FC1-4	0.008647	0.000008	1.467371	0.000024	0.000371	0.000003	0.282180	0.000007	-21.41	0.26
FC1-5	0.008669	0.000008	1.467354	0.000026	0.001148	0.000004	0.282177	0.000010	-21.51	0.35
FC1-6	0.008637	0.000011	1.467467	0.000029	0.000672	0.000002	0.282180	0.000014	-21.41	0.49
FC1-7	0.008667	0.000014	1.467340	0.000029	0.001109	0.000010	0.282171	0.000009	-21.70	0.33
FC1-7	0.008648	0.000012	1.467378	0.000043	0.001107	0.000002	0.282175	0.000011	-21.58	0.40
FC1-8	0.008657	0.000012	1.467436	0.000032	0.001182	0.000000	0.282181	0.000013	-21.37	0.46
Average (this stud	*0.008655*		*1.467388*		*0.001033*		*0.282180*	*±13 (2 SD)*	*-21.40*	*0.24*
Accepted value (Woodhead and Hergt, 2005)					**0.001262**		**0.282184**	**0.000016**	**-21.25**	**0.57**
TEM-2.1	0.008647	0.000011	1.467351	0.000029	0.000610	0.000015	0.282657	0.000009	-4.54	0.30
TEM-2.2	0.008670	0.000014	1.467414	0.000031	0.000693	0.000004	0.282665	0.000010	-4.26	0.37
TEM-2.3	0.008641	0.000016	1.467397	0.000039	0.001206	0.000005	0.282671	0.000013	-4.03	0.45
TEM-2.4	0.008655	0.000016	1.467371	0.000032	0.001456	0.000003	0.282689	0.000018	-3.39	0.62
TEM-2.5	0.008670	0.000012	1.467373	0.000031	0.001176	0.000024	0.282686	0.000010	-3.50	0.36
TEM-2.6	0.008670	0.000013	1.467330	0.000029	0.001145	0.000008	0.282686	0.000010	-3.50	0.36
TEM-2.7	0.008656	0.000015	1.467376	0.000027	0.000967	0.000032	0.282683	0.000010	-3.62	0.34
TEM-2.8	0.008661	0.000010	1.467399	0.000029	0.000989	0.000002	0.282695	0.000010	-3.18	0.34
TEM-2.9	0.008637	0.000014	1.467373	0.000030	0.001498	0.000001	0.282683	0.000010	-3.61	0.35
Average (this stud	*0.008656*				*0.001082*		*0.282679*	*±25 (2 SD)*	*-3.74*	
Accepted value (Woodhead and Hergt, 2005)					**0.00109**		**0.282686**	**± 8**	**-3.50**	
R33-1	0.008659	0.000015	1.467406	0.000042	0.001760	0.000046	0.282761	0.000014	-0.85	0.49
R33-2	0.008645	0.000017	1.467409	0.000034	0.002019	0.000010	0.282756	0.000011	-1.02	0.38
R33-3	0.008644	0.000011	1.467389	0.000030	0.000632	0.000009	0.282755	0.000010	-1.07	0.35
R33-4	0.008634	0.000016	1.467323	0.000036	0.001805	0.000042	0.282744	0.000014	-1.46	0.50
R33-5	0.008676	0.000016	1.467520	0.000036	0.000927	0.000025	0.282770	0.000013	-0.53	0.47
R33-6	0.008702	0.000020	1.467365	0.000035	0.001582	0.000053	0.282763	0.000011	-0.79	0.38
R33-7	0.008655	0.000011	1.467402	0.000032	0.001264	0.000003	0.282756	0.000009	-1.02	0.32
Average (this stud	*0.008659*				*0.001427*		*0.282758*	*±16 (2 SD)*	*-0.96*	
Accepted value (Fisher et al., 2014)					**0.001989**	**0.008690**	**0.282764**	**±14**	**-0.80**	

References

Fisher, C.M., Vervoort, J.D., DuFrane, S.A., 2014. Accurate Hf isotope determinationsof complex zircons using the "laser ablation split stream" method. Geochemistry Geophysics Geosystems 15, 121–139. http://dx.doi.org/10.1002/2013GC004962.

Sláma, J., Ko˘sler, J., Condon, D. J., Crowley, J. L., Gerdes, A., Hanchar, J. M., Horstwood, M. S. A., Morris, G. A., Nasdala, L., Norberg, N., Schaltegger, U., Schoene, B., Tubrett, M. N., Whitehouse, M. J., 2008. Plešovice zircon—A new natural reference material for U–Pb and Hf isotopic microanalysis. Chemical

Woodhead, J., Hergt, J., 2005. A preliminary appraisal of seven natural zircon reference materials for in situ Hf isotope determination. Geostandards and Geoanalytical Research 29, 183–195. doi:10.1111/j.1751-908X.2005.tb00891.x.

Supplementary Table 2. Complete Hf isotopic compositions of sample zircons.

Supplementary Table 2. Complete Hf isotopic compositions of sample zircons.

Analysis Name	$^{174}Hf/^{177}Hf$	1SE	$^{178}Hf/^{177}Hf$	1SE	$^{176}Lu/^{177}Hf$	1SE	$^{176}Hf/^{177}Hf$	1SE
1.1	0.008693	0.000015	1.467362	0.000039	0.000610	0.000008	0.282766	0.000013
2.1	0.008631	0.000010	1.467423	0.000035	0.000734	0.000016	0.282763	0.000011
3.1	0.008654	0.000026	1.467295	0.000058	0.000912	0.000023	0.282711	0.000017
4.1	0.008656	0.000011	1.467345	0.000031	0.000407	0.000002	0.282716	0.000010
5.1	0.008613	0.000015	1.467416	0.000034	0.000914	0.000026	0.282712	0.000012
6.1	0.008689	0.000017	1.467364	0.000036	0.001347	0.000002	0.282690	0.000012
7.1	0.008668	0.000025	1.467343	0.000046	0.000496	0.000006	0.282731	0.000022
8.1	0.008649	0.000027	1.467384	0.000058	0.001781	0.000056	0.282756	0.000020
9.1	0.008740	0.000020	1.467496	0.000055	0.001245	0.000081	0.282817	0.000014
11.1	0.008668	0.000010	1.467412	0.000027	0.000766	0.000041	0.282749	0.000009
12.1	0.008669	0.000011	1.467411	0.000035	0.000400	0.000001	0.282746	0.000013
13.1	0.008691	0.000029	1.467394	0.000049	0.003011	0.000047	0.282797	0.000022
14.1	0.008673	0.000037	1.467362	0.000071	0.002163	0.000013	0.282694	0.000019
15.1	0.008674	0.000010	1.467343	0.000030	0.000662	0.000004	0.282755	0.000009
16.1	0.008681	0.000016	1.467356	0.000035	0.000395	0.000003	0.282732	0.000015
17.1	0.008632	0.000013	1.467345	0.000033	0.000914	0.000001	0.282741	0.000009
18.1	0.008682	0.000023	1.467360	0.000042	0.001804	0.000065	0.282763	0.000016